EXPLORING AND CORRECTING MOTION IN RESTING-STATE FUNCTIONAL MAGNETIC RESONANCE IMAGES OF CONGENITAL HEART DISEASE PATIENTS

by

Jenna Marie Schabdach

B. S. Electrical Engineering, Drexel University, 2016

M. S. Electrical Engineering, Drexel University, 2016

M. S. Biomedical Informatics, University of Pittsburgh, 2018

Submitted to the Graduate Faculty of

the Department of Biomedical Informatics in partial fulfillment

of the requirements for the degree of

Doctor of Philosophy

University of Pittsburgh

2019

UNIVERSITY OF PITTSBURGH

SCHOOL OF MEDICINE

This dissertation was presented

by

Jenna Marie Schabdach

It was proposed on

June 27, 2019

and approved by

Dr. Douglas Landsittal, Department of Biomedical Informatics

Dr. Ashok Panigrahy, Department of Biomedical Informatics

Dr. Gregory Cooper, Department of Biomedical Informatics

Dr. Rafael Ceschin, Department of Pediatric Radiology, Children's Hospital of Pittsburgh of UPMC

Dissertation Director: Dr. Douglas Landsittal, Department of Biomedical Informatics

EXPLORING AND CORRECTING MOTION IN RESTING-STATE FUNCTIONAL MAGNETIC RESONANCE IMAGES OF CONGENITAL HEART DISEASE PATIENTS

Jenna Marie Schabdach, PhD

University of Pittsburgh, 2019

INSERT ABSTRACT HERE

TABLE OF CONTENTS

1.0 INTRODUCTION

Every year, approximately 1.35 million children are born with a congenital heart defect [van der Linde et al., 2011]. Congenital heart defects (CHDs) have many presentations, and all cause problems in a patient's heart structure and the structure of the surrounding vessels. It has been found that the development of cardiac problems in utero is often linked to problems in patient neurodevelopment. Research in the area of cardiac and neurodevelopment has often focused on identifying these problems in younger populations. However, treatment of CHDs has evolved over the past fifty years with the result that many CHD patients live to adulthood: it is estimated that about 12 to 34 million adults are living with CHD. Researchers are now starting to investigate the relationships between CHD and neurocognitive disorders in this aging population. Eventually, clinicians will be able to develop a lifespan approach to managing CHD and neurocognitive disorders, but we as a community are still in the data-gathering stage of this research.

The process for diagnosing CHDs is relatively established, but the process for objectively identifying neurocognitive disorders is less certain. Psychologists have developed and validated surveys to estimate a patient's neurocognitive status. These surveys vary as the child ages. Initially, a parent fills out the survey on behalf of his infant or toddler child. When the child has reached certain developmental milestones, the parent and child might both fill out different portions of a different survey. At some point, the child can fill out his own survey. Psychologists may meet with the patient and his parents to determine a diagnosis. All of these methods are highly subjective.

A more objective methods for identifying neurocognitive disorders are evolving in the medical imaging domain. Resting-state functional magnetic resonance imaging (rs-fMRI) measures the blood oxygen level dependent signal in an organ or organ system. Effectively,

an rs-fMRI can measure the amount f activity in underlying networks connecting different areas of the brain. The study of these networks is called functional connectivity analysis, and it is an invaluable tool for evaluating a patient's neurodevelopmental status.

To gather enough data to fully evaluate these networks, a series of image volumes must be acquired over a period of several minutes. In a standard rs-fMRI, one new image volume is obtained approximately once every two to three seconds. To gather high quality data on such a short timescale, the rs-fMRI suffers from two major limitations: rs-fMR images have low physical resolution and are highly susceptible to motion. The first limitation can be addressed by obtaining an MR image with high physical resolution and registering the rs-fMRI to this structural image, but the second limitation requires the patient to remain as still as possible for the entire duration of the scan. This task is particularly difficult for populations of certain ages and populations who suffer from neurocognitive disorders. As a result, it is common for an image from a member of one of these populations to contain too much motion to be used in clinical or research applications.

Various clinical, behavioral, and technical protocols have been developed in an attempt to prevent patient motion from impacting the acquired rs-fMR image. Sedation can be used to immobilize a patient during a scan, but requires additional personal to perform safely and involves a greater time commitment from the patient. Sedation is also not recommended for use in young children and fetal patients. Behavioral and educational techniques can be employed to prepare a patient for stressors he may experience during an rs-fMRI scan, but these approaches do not prevent the patient from moving out of boredom, discomfort, or distress. Several groups have developed techniques to compensate for motion as an image is acquired, but these techniques often require additional MR compatible equipment and can only be utilized during the scan. After a rs-fMR image is acquired, however, it is possible to reduce the positional effects of motion in the image sequence.

Many methods have been developed to mitigate the effects of motion after the rs-fMRI is acquired. While different post-acquisition motion correction pipelines utilize different processing techniques, they begin with global volume registration. Global volume registration is the process used to align all volumes in a rs-fMRI sequence into the same physical space. Traditionally, all volumes in the sequence are registered directly to one volume. This ap-

proach can be effective in images where the subject remains relatively still throughout the duration of the scan, but is not as successful in images containing high quantities of patient movement.

We have developed an alternative volume registration framework which takes into account the spatiotemporal relationships between sequential volumes in the rs-fMRI sequence and uses these relationships during the registration process. We have demonstrated the feasibility of this technique on a high-motion neonatal brain rs-fMRI data set and compared it to the traditional registration framework. Herein, we evaluate it further in the context of a complete motion correction pipeline across healthy and CHD populations at various stages of life.

While correcting motion within an rs-fMRI is important both for clinical use and research applications, we are also interested in the motion itself. In addition to evaluating a global volume registration framework in the context of a fully motion correction pipeline, we also investigate the relationships between a patient's motion and their clinical outcomes, specifically to further the study of congenital heart disease (CHD) across the lifetime of the patient.

Our aims for this project are as follows:

- **Aim 1.** Evaluate the impact of global volume registration within a complete motion correction pipeline in simulated and clinical data.
- **Aim 2.** Study the motion patterns in the different populations to formally describe age-group or clinical status related motion patterns.
- **Aim 3.** Employ machine learning techniques to (a) measure the impact of motion on image harmonization in multi-center studies, and (b) evaluate the relationship between motion and cognitive, clinical, and behavioral outcomes of CHD patients.

We have a large set of neurological rs-fMRIs for both healthy control and CHD neonatal, preadolescent, and adult subjects. We also have a set of neurological and placental rs-fMRIs for fetal patients. We will apply both the tradition and novel registration frameworks to all images in our different cohorts and evaluate the impact of each framework on each image after passing it through a complete motion correction pipeline. The original and registered images will be used to address the aims discussed in this chapter.

The remainder of this document is laid out as follows. In Chapter 2, we discuss congenital heart disease, its relationship with neurological conditions, and methods for evaluating neurological conditions. We elaborate on the use of resting-state functional magnetic resonance images (rs-fMRIs) for investigating functional brain networks in Chapter 3. Chapter 4 transitions into methods for analyzing MRIs, machine learning techniques, and our approach to statistical analysis. We discuss the data we use in Chapter 5, and explain the experiments we plan to do in Chapter 6. Chapters 7 and 8 contain preliminary results and a discussion of these results from our initial study comparing two registration techniques in a neonatal dataset.

2.0 NEURODEVELOPMENT, CONGENITAL HEART DISEASE, AND FUNCTIONAL CONNECTIVITY

2.1 CONGENITAL HEART DEFECTS

Congenital heart defects and congenital heart disease (CHD) both refer to defects in the heart or the vessels around the heart which formed during fetal development. Heart defects affect how blood moves into, through, and away from the heart. CHD can affect any combination of heart chambers and blood vessels with varying degrees of severity. The lesions prevent the cardiopulmonary system as a whole from functioning correctly, but pinpointing and treating the defects effectively can be a complex process.

There are a number of genetic and environmental factors associated with different presentations of CHD [Mozaffarian et al., 2016]. Genetic conditions such as Down syndrome, Turner syndrome, 22q11 deletion syndrome, Williams syndrome, and Noonan syndrome are associated with different CHD presentations. Maternal behaviors such as smoking and binge drinking are known to cause heart problems in the fetus. Other maternal risk factors are obesity, folate deficiency, and living at a high altitude. Paternal exposure to phthalates, anesthesia, sympathomimetic medications, pesticides, and solvents may increase the risk of the fetus for developing CHD. While there are quite a few factors in this list, there are many CHD cases whose causes are unknown.

The process of diagnosing CHD can begin before birth. A specialized ultrasound test called fetal echocardiography can detect heart abnormalities as early as the second trimester of the pregnancy. Additional tests, such as amniocentesis and follow-up ultrasounds may be needed to determine treatment options. Generally, severe CHD cases present and are detected at earlier stages, but minor defects may not become apparent until the patient is

Table 15-3. Estimated Prevalence of Congenital Cardiovascular Defects and Percent Distribution by Type, United States, 2002* (in Thousands)

	Prevalence, n			Percent of Total		
Type	Total	Children	Adults	Total	Children	Adults
Total	994	463	526	100	100	100
VSD†	199	93	106	20.1	20.1	20.1
ASD	187	78	109	18.8	16.8	20.6
Patent ductus arteriosus	144	58	86	14.2	12.4	16.3
Valvular pulmonic stenosis	134	58	76	13.5	12.6	14.4
Coarctation of aorta	76	31	44	7.6	6.8	8.4
Valvular aortic stenosis	54	25	28	5.4	5.5	5.2
TOF	61	32	28	6.1	7	5.4
AV septal defect	31	18	13	3.1	3.9	2.5
TGA	26	17	9	2.6	3.6	1.8
Hypoplastic right heart syndrome	22	12	10	2.2	2.5	1.9
Double-outlet right ventricle	9	9	0	0.9	1.9	0.1
Single ventricle	8	6	2	0.8	1.4	0.3
Anomalous pulmonary venous connection	9	5	3	0.9	1.2	0.6
Truncus arteriosus	9	6	2	0.7	1.3	0.5
HLHS	3	3	0	0.3	0.7	0
Other	22	12	10	2.1	2.6	1.9

Average of the low and high estimates, two thirds from low estimate.[24]ASD indicates atrial septal defect; AV, atrioventricular; HLHS, hypoplastic left heart syndrome; TGA, transposition of the great arteries; TOF, tetralogy of Fallot; and VSD, ventricular septal defect.

*Excludes an estimated 3 million bicuspid aortic valve prevalence (2 million in adults and 1 million in children).

†Small VSD, 117 000 (65 000 adults and 52 000 children); large VSD, 82 000 (41 000 adults and 41 000 children).

Source: Data derived from Hoffman et al.[24]

Figure 1: Table of prevalences of congenital heart defects borrowed temporarily from [Mozaffarian et al., 2016].

older.

The incidence of CHD in live births vary across countries and continents. The United States reports approximately 4-10 CHD case per 1,000 live births. Europe and Asia see about 6.9 and 9.3 CHD cases per 1,000 live births [Mozaffarian et al., 2016]. In China, the incidence of CHD ranges from 8.98 to 11.1 per 1,000 live births [Zhao et al., 2019] [Qu et al., 2016]. A pair of studies from Iran report incidences of 8.6 and 12.3 per 1,000 live births, and the studies note that they were performed in different geographical locations with different populations within the country [Nikyar et al., 2011] [Rahim et al., 2008]. One report from Dharan reports an incidence of 5.8 per 1,000 patients admitted to a tertiary care hospital over a 12 month period [Shah et al., 2008]. A study of newborns at one hospital in New Delhi, India claims an incidence of 3.9 per 1,000 live births, though this rate may be a poor estimate as there is a significant delay between patient birth and referral to a cardiac center in India [Khalil et al., 1994] [Saxena, 2005].

These incidence rates should be analyzed with some caution. In many cases, the reported

rates were based on medical records. Medical records are not always correct. Additionally, the only way for a person to have a correct medical record is for him to go to a medical center. Not everyone who has CHD is able to seek medical help, often because of their geographical locations or their income. Even if a patient is able to seek medical help, the availability of proper cardiac care varies between and within countries.

As screening tools become more effective and more widespread, it is expected that incidence rates will increase as defects are detected earlier. Generally, the earlier a defect is detected, the earlier it can be treated. Early detection and treatment means more CHD patients will live to adulthood. Currently, Webb et al. estimate that at least 12 to 34 million adults have CHD, and this number is expected to increase [Webb et al., 2015].

A breakdown of prevalence rates of some of the most common lesion types can be seen in Figure 1.

Once a patient is diagnosed with one of these defects, the specific nature of his case must be clearly documented. The documentation of CHD using the International Classification of Diseases, Ninth Revision, Clinical Modification (ICD-9-CM) has 25 high level codes representing various presentations of CHD, but these codes used on their own are often not sufficient for describing a patient's true condition [Mozaffarian et al., 2016]. Additional ICD-9-CM codes should be used to communicate the finer details of a patient's condition.

The financial burden of CHD varies depending on the defect. Certain defects require complex, expensive surgical repairs while others can be treated with less expensive approaches [Mozaffarian et al., 2016]. The burden of CHD across the globe was outlined by Webb et al. Their figure illustrating the prevalence of CHD and the availability of funds with which to treat it can be see in Figure 2. As the overall mortality of CHD declines, the burden of CHD is expected to increase [Mozaffarian et al., 2016].

Unfortunately, the cost of treating CHD alone is not the only burden a patient must undergo. Patients with CHD are also at increased risk for heart failure and infections [Mozaffarian et al., 2016]. Children with CHD are at 19-fold risk for stroke compared to their healthy counterparts [Fox et al., 2015]. Giang et al performed a study comparing the prevalence of cardiac conditions in patients with and without CHD born between 1970 and 1993 in Sweden. They found that patients who had a CHD diagnosis were at about eight

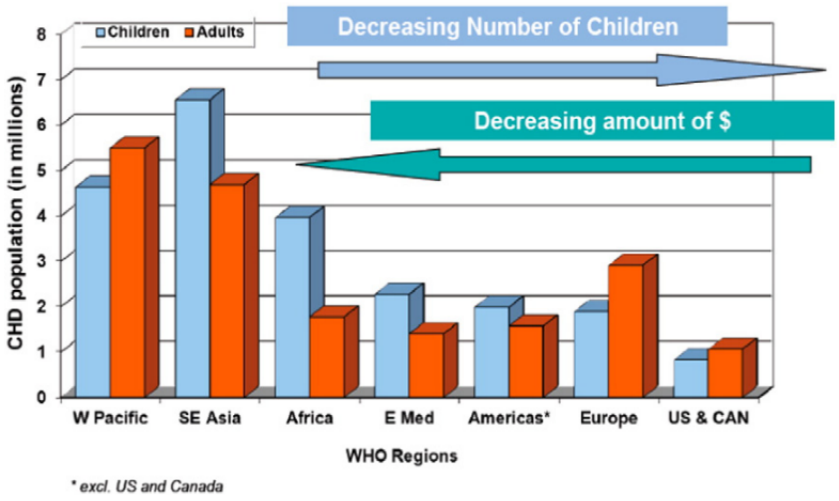

Figure 2: Estimated CHD burden in World Health Organization (WHO) regions using incidence rates of approximately 12/1000 and 4/1000 in children and adults, respectively [Webb et al., 2015].

times higher risk for intracerebral hemorrhage and subarachnoid hemorrhage than their non-CHD counterparts. The CHD patients were also more likely to suffer from arrhythmia and heart failure.

2.2 CHD AND NEUROCOGNITIVE DISORDERS

Cardiac conditions are not the only complications CHD must deal with. Recently, researchers have found that there is a relationship between CHD and neurocognitive disorders.

Early research in this area focuses on the neurodevelopmental status of neonatal patients pre- and post-surgical intervention. One theory was that some factor or factors in the surgical intervention caused brain injuries in the patients. This idea proved to be inaccurate when researchers began detecting neurological malformations in utero.

In a systematic review of available literature regarding prenatal and postnatal presurgical

CHD cases and neurodevelopmental outcomes, Mebius et al. identify two theories about the causality of neurodevelopmental delays and CHD [Mebius et al., 2017]. The first theory is that abnormalities in the cardiac system prevent the developing brain from receiving enough oxygen and nutrients, which disrupts prenatal brain development. The second theory is that faulty genetic pathways used during both cardiac and brain development cause both conditions to co-occur.

However, a third theory has begun to emerge. Since the combination of CHD and abnormal neurodevelopmental outcomes can be traced back to prenatal development, researchers investigated other factors related to prenatal brain oxygenation. During the prenatal period, a fetus receives oxygen from the mother via the placenta. Mebius et al. found 11 articles related to bloodflow through the umbilical artery. Though these articles have contradictory results, the role of the placenta in CHD and brain development cannot yet be discounted.

Survival of CHD patients to adulthood has increased from 10% to 90% over the last several decades. The impact of the combination of CHD and neurological conditions is being explored. The aging of the CHD population has also sparked interest in the relationships between CHD and adult-stage neurological disorders such as dementia and Alzheimer's.

2.3 IDENTIFYING NEUROCOGNITIVE DISORDERS

2.3.1 PATIENT SURVEYS

Surveys known to be used for studying the relationship between CHD and neurodevelopment are

- National Institute of Health Toolbox (3 - 85 years): "Performance tests of cognitive, motor, and sensory function and self-reported measures of emotional function for adults and children in the general population and those living with a chronic condition".
- Sue Beers (4 - 18 years [not inclusive of 18 years]): WASI-II, NEPSY-2, WRAML-2, D-KEFS, WISC-IV, Grooved Pegboard, BRIEF, Beery-Buktenica VMI, ASRS, Conners-3, BASC-II, ABAS-II, PedsQL General, PedsQL Cardiac, Pictoral Scale Self Perception

Profile.

- SVR-III NDT (9 - 13 years [not inclusive of 13 years]): WIAT, NEPSY, WRAML, D-KEFS, WISC-V, Grooved Pegboard, BRIEF, Beery-Buktenica VMI, ASRS, Conners ADHD Index, BASC-II, ABAS-3, PedsQL General, PedsQL Cardiac
- Bayley Scales of Infant and Toddler Development -III (1 - 24 months): Subtests include cognitive, language, social-emotional, motor, and adaptive behavior tests [Mebius et al., 2017].
- Battelle Developmental Inventory (Birth - 8 years [not inclusive of 8 years]): Subsets include cognition, communication, social-emotional development, physical development, and adaptive behavior.
- Developmental Assessment of Young Children (Birth - 6 years [not inclusive of 6 years]): Subtests include cognition, communication, social-emotional development, physical development, and adaptive behavior.
- Preschool Language Scale + Receptive-Expressive Emergent Language (Birth - 3 years): Total language, auditory comprehension, expressive communication, articulation, receptive language, expressive language, and inventory of vocabulary words.
- Peabody Developmental Motor Scales (Birth - 5 years): Subtests include reflexes, stationary, locomotion, object manipulation, grasping, visual-motor integration

2.3.2 NEUROLOGICAL IMAGES

When an area of the brain is active, it uses more oxygen than the surrounding regions. Combinations of brain regions which are active at the same time are called neuronal networks. The idea of a neuronal network which operated when a person is at rest was proposed in 2001, and then confirmed in 2003 [Raichle et al., 2001] [Greicius et al., 2003]. Resting-state networks are recorded using resting-state functional magnetic resonance images (rs-fMRIs). rs-fMRIs are sequences of image volumes acquired over a period of a few minutes while the patient is in a task-free state. The image volumes themselves have relatively low spatial resolution when compared to structural MRIs, but their temporal resolution is significantly higher as a new volume is acquired every two to three seconds. Each volume records the blood oxygen level dependent (BOLD) signals within the brain at that point in time.

The BOLD signals in rs-fMRI image sequences are analyzed using a process called functional connectivity analysis. Functional connectivity analysis identifies patterns and networks of brain activity. Because the patient is not performing a specific task during a rs-fMRI acquisition, these resting-state networks have the potential to reveal valuable information about a patient's neurodevelopmental status. Some functional connectivity analysis studies have lead to the discoveries of links between specific disruptions in these naturally occurring networks and neurodevelopmental diseases such as autism and attention deficit hyperactivity disorder [Assaf et al., 2010] [Zang et al., 2007]. With further refinements of both acquisition techniques and characterization of these functional networks, clinicians may be able to use rs-fMRI to evaluate the neurodevelopmental status of CHD patients and to identify patients who may benefit from certain therapies or neuroprotective interventions.

The next chapter will address the challenges of using rs-fMRIs as a tool for diagnosing CHD.

3.0 RS-FMRIS AND PATIENT MOTION

This chapter covers one of the most prominent challenges in using rs-fMRIs: patient motion. These topics include sources of motion, current methods for preventing and managing motion in rs-fMRIs, quantifying motion, and usability criteria for using images corrupted by motion.

3.1 SOURCES OF MOTION IN MEDICAL IMAGES

During every medical imaging scan, the patient will naturally perform small, automatic movements due to regular bodily functions. Minuscule movements caused by cardiac activity may disrupt scans with high spatial resolution or with high sensitivity to the movement of blood molecules. Larger movements caused by respiration result in motion artifacts in images of the thoracic and abdominal cavities.

Other motions occur on a larger and more conscious scale. It is important to note that different populations may exhibit more of certain macro-motions than others. The patient may fidget or shift his gaze when he becomes bored in the scanner. If the patient falls asleep during a scan, there may be slight movement as the body relaxes and retenses if the patient wakes. Certain MRI protocols are known to produce loud sounds: during one of these protocols, the patient may become surprised and react by jumping. Additionally, clausterphobic patients or patients who feel secure around specific people who are not allowed in the scanner room may become agitated.

3.2 STRUCTURE OF A RS-FMRI

A rs-fMRI scan produces a four dimensional image series. The first three dimensions are length, width, and depth and encompass the physical space occupied by the patient's head. The information in these three dimensions is interpreted as a three dimensional, volumetric image. The fourth dimension is time. The temporal dimension interacts with the spatial dimensions such that the contents of that image volume change with time.

rs-fMRIs are discrete representations of continuous data. A new image volume of the patient's brain is acquired every two to three seconds. The image volume is composed of a three dimensional version of a pixel called a voxel (volume element). Just as the "distance" between each image volume encompasses a certain amount of time, each voxel encompasses a small volume of physical space. The transformations between the continuous physical and temporal dimensions and the discrete physical and temporal dimensions are the spatial and temporal resolutions.

An rs-fMRI is considered to have relatively low spatial resolution but high temporal resolution. The physical size of a single voxel seems small at about 4 mm^3, but this resolution is not granular enough to capture details about activity within small structures of the brain. The activity information recorded during a rs-fMRI must be combined with the detailed anatomic information from a structural MRI to know precisely which areas of the brain are active at each point in time. A structural MRI volume takes much longer to acquire than a rs-fMRI volume, which can be obtained every two to three seconds. Unfortunately, the patient's position and neural activity can change faster than the image volume can be acquired. As a result, a temporal resolution of two to three seconds is not fast enough to actively compensate for sources of noise which confound the BOLD signal.

3.3 EFFECTS OF MOTION

Due to their low spatial and high temporal resolutions, rs-fMRIs are highly susceptible to all types of motion outlined in the previous section. The effects of motion on rs-fMRIs can

be clearly divided into two categories: the effect on patient position and the effect on the recorded BOLD signal.

3.3.1 Positional Effects of Motion

The smallest movement can alter the position of the patient enough to cause the voxels to record signals from different brain regions and tissue types. The technique used for analyzing rs-fMRIs, called functional connectivity analysis, does not know anything about changes in patient position during the scan. It assumes that the contents of one voxel at two different time points both contain signal from a single point in the brain. This assumption is vital to the networks of activity the technique infers.

The effect of motion on patient position is measured in terms of the difference in position between temporally neighboring image volumes. The difference in position is determined using metrics calculated by performing rigid volume registration on the two volumes. In rigid volume registration, one volume is chosen as the reference volume and the other is considered the moving volume. The reference volume remains stationary while the moving volume is translated and rotated in three-dimensional space on top of it. The registration is considered successfully complete when the position of the patient in the moving volume matches the position in the reference volume.

The moving volume can undergo linear or nonlinear transformations. Linear transformations include translation, rotation, and affine transformations along all three spatial dimensions as well as a scaling factor. These transformations move the image volume as a whole: all voxels in the moving image remain in the same location relative to their neighbors. On the other hand, nonlinear transformations have the ability to warp the contents of the moving volume so that it better matches the contents of the reference volume. Nonlinear transformations are more complex than linear transformation. They involve additional image processing steps such as smoothing and interpolation.

Even in cases when nonlinear transformations are used, the registration process begins with the translation and rotation transformations. The three translation and three rotation parameters used to achieve the best alignment are used to calculate the positional change

between the image volumes. The positional change between temporally neighboring volumes is called the framewise displacement (FD).

Several researchers have proposed different methods for calculating the FD. Power et al., Jenkinson et al., and Dosenbach et al. each propose a slightly different method for calculating the FD [Power et al., 2012] [Jenkinson et al., 2002] [Dosenbach et al., 2017]. All three FD calculations produce correlated metrics: the FD metric proposed by Power et al. produces measurements approximately twice as large as the metric proposed by Jenkinson et al., and Dosenbach et al. reported a high correlation between their FD and Powers FD [Yan et al., 2013b] [Dosenbach et al., 2017]. Herein, we use Power et al.'s version of the FD metric.

3.3.2 Signal Effects of Motion

In addition to changing the recorded position of the subject, it impacts the established spin gradients, which introduces artifacts into the image sequence.

During an ideal MRI scan, the patient is sitting in the scanner and all molecules are aligned with the primary magnetic field B_0 in a relaxed state. Then, an radiofrequency (RF) pulse is applied to the field. The purpose of the pulse is to excite the molecules in a certain volume of physical space to orient the molecules to align to a secondary field in a different plane. When the pulse ends, the molecules precess back to their orientation in B_0. As they do, their small magnetic fields induce electric currents on the RF coil. The currents are received by the scanner as signals in frequency space. The volume of the space intended to be excited is known, and the signal produced by the induced electric current is used in conjunction to reconstruct the image in voxel space.

However, when the patient moves, the volume of space which was thought to be excited is not actually excited: some other volume of space, which may or may not overlap with the intended volume of space, is excited instead. Because the MRI scanner has no way to know this assumption is not true, it does not know that not all of the molecules in its intended area are relaxed and correctly aligned to the B_0 field at the end of the RF pulse. The scanner proceeds with the next RF pulse, which tries to excite "relaxed molecules" which are not

actually relaxed. As a result, the signals produced in the second RF pulse are different than they should be. For example, signals that are smaller than they should be result in dark shadows within motion affected frames of the sequence.

These effects of motion are more difficult to measure than the positional effects. They occur because motion disrupts the magnetic spin gradients present in the patient during the scan. The spin gradients need time to recover to the correct magnetic field orientation, and up to eight to ten seconds may pass before the recovery is complete [Power et al., 2014]. While the spin gradients are reorienting, the recorded BOLD signal will vary more than usual between temporally neighboring volumes.

There are few metrics to measure the change in BOLD signal between image volumes. In 2010, Smyser et al. developed a metric called DVARS, which measures the temporal derivative of the root mean squared variance over the voxels between two volumes [Smyser et al., 2010]. Power et al. explain the steps to calculate DVARS in a separate study [Power et al., 2012]. The DVARS value is calculated in two steps. The first step uses backward differences to approximate the derivative of the BOLD signal change between volumes J_i and J_{i-1} at every point $\vec{x}$:

$$\frac{\partial}{\partial t} J_i(\vec{x}) \approx J_i(\vec{x}) - J_{i-1}(\vec{x}). \tag{3.1}$$

The second step calculates the root mean square of the approximated derivatives for all N points $\vec{x}$ contained in both image volumes:

$$DVARS(J_i) = \sqrt{\frac{1}{N} \sum_{\vec{x} \in J_i, J_{i-1}} \left(\frac{\partial}{\partial t} J_i(\vec{x}) \right)^2}. \tag{3.2}$$

DVARs measures the change in BOLD signal intensity, which is highly related to motion-induced spin gradient changes.

3.4 MOTION PREVENTION

Various techniques and protocols have been developed to prevent patients from moving during the image acquisition process. Not all of these techniques are suitable for all patient populations, and some techniques have been designed specifically for certain populations.

3.4.1 Sedation

Sedation can be used to help a patient tolerate an MRI scan. Murphy and Brunberg retrospectively analyzed seven weeks of data from the MR department and found that 14.2% of their adult patients required some form of sedation [Murphy and Brunberg, 1997]. In a study about claustrophobia and MR acquisitions, Dewey et al. report that out of 55,734 patients who underwent MRI scans, a total of 1,004 patients experienced claustrophobia and 610 of these patients required intravenous sedation before their scans [Dewey et al., 2007]. Even though sedation allowed the patients mentioned in this paragraph to undergo an MRI scan, the authors of both studies note that sedation can result in adverse events and advise the reader to avoid patient sedation if possible.

Sedation can be used with pediatric patients, though the risks are more significant than with adult patients. Studies have shown that sedation for pediatric imaging can lead to hypoxemia and inappropriate sedation levels during image acquisition [Malviya et al., 2000]. Pediatric patients can also expect "motor imbalance and gastrointestinal effects," as well as agitation and restlessness for a period of hours after waking from sedation.

A report from the American Academy of Pediatrics and the American Academy of Pediatric Dentistry outlines the minimum set of criteria needed for a pediatric patient to be sedated for a procedure [Coté and Wilson, 2016]:

- The patient must be a suitable candidate for sedation based on their medical history and medical needs.
- The patient's health status must be evaluated and verified by the sedation team prior to the procedure.
- Informed consent must be obtained prior to the procedure.

- Instructions for what to expect and how to transport the patient home safely must be provided to the patient's responsible adult.
- At least one responsible adult must be with the patient at the medical facility, though the report recommends that two adults are present for patients who travel to and from the facility using car seats. This practice ensures that one adult can monitor the patient after the procedure while the other adult drives.
- The patient's food and drink intake prior to the procedure should be taken into account to minimize the risk of pulmonary aspiration.
- The clinician administering the sedation must have immediate access to emergency facilities, personnel, and equipment, and should monitor the patient for adverse events including respiratory events, seizures, vomiting, and allergic reactions.
- There must be a clear protocol outlined for immediately accessing these emergency services.
- Emergency equipment and drugs appropriate for the patient's size and age must be immediately available in case the patient needs to be resuscitated.
- The information about the procedure must be correctly documented.
- The facility should have a dedicated recovery area, and the status of the patient should be recorded when he is discharged. The patient should not be discharged if his level of consciousness and oxygen saturation do not meet recognized guidelines.
- The patient may be held at the facility for prolonged monitoring after the procedure.

This report clearly states that the levels of monitoring suggested above should serve as minimum levels of involvement: clinicians should increase patient monitoring as needed for complex cases. Rutman has a similar and detailed perspective on patient monitoring during and after sedation, adding that two independent medical personnel should be present during the scan and one should be present until the patient is discharged [Rutman, 2009]. Rutman also notes that all sedation and monitoring equipment must be MR compatible, which is a simple but important safety constraint. This constraint makes sedation less advisable if the appropriate equipment is not available.

Sedation in neonatal and infant populations is not recommended. The U. S. Food and Drug Administration (FDA) issued a warning in late 2016 about repeated use of sedation or

general anesthesia for patients under three years of age or for pregnant women during their third trimester [United States Food and Drug Administration, 2016]. The warning states that while a single, relatively short exposure to sedative and anesthetic drugs is unlikely to impact the patient, the effects of prolonged exposure to these drugs are still being studied. Studies of sedative and anesthetic drugs in multiple animal models have shown that these drugs can lead to loss of nerve cells in the brain when the animals undergo prolonged, repeated exposure to them during period of brain development. More data is needed to determine if this effect translates to humans.

3.4.2 Education, Distraction, and Behavioral Techniques

Educational material can be used to help the patient understand what to expect during an MRI scan as well as to teach the patient different behavioral coping strategies. The education materials can be used either before or upon arrival at the imaging facility.

Most of the formal literature focuses on educational, distraction, and behavioral techniques to use during pediatric MRI scans. Many of the following approaches could be adapted for use with adults.

In a review of the available literature, Alexander found several commonly used techniques to educate, comfort, and distract pediatric patients during radiology procedures [Alexander, 2012]. Tools such as educational coloring books and short videos can expose patients to the types of equipment they can expect to see using a familiar, engaging medium. Pediatric patients can learn coping strategies to employ during the scan such as breathing techniques, imagery, and positive statements. Alexander notes that allowing a pediatric patient to choose a behavioral coping strategy gives the patient a sense of control and may encourage the patient to cooperate during the MRI acquisition.

Mock scanners and MRI simulators can also help the patient feel more comfortable during the scan. Barnea-Goraly et al. showed that both a commerical MRI simulator and a low-tech mock scanner desensitized pediatric patients between four and ten years of age to the MRI scanner with the results that 92.3% of the acquired images could be used in high-resolution anatomical studies [Barnea-Goraly et al., 2014].

Several groups have investigated the role of auditory and visual distraction during an MRI acquisition. Headphones with music and stories or MR compatible video goggles can distract patients from the tedium of the scan [Alexander, 2012] [Barnea-Goraly et al., 2014] [Harned and Strain, 2001]. Khan et al. found that a relatively simple moving light show can be helpful in distracting younger patients [Khan et al., 2007]. Garcia-Palacios et al. performed a case study comparing the efficacy of music and immersive virtual reality tools as distractions during a mock scan [Garcia-Palacios et al., 2007]. They suggest that immersive virtual reality may help decrease patient anxiety during a scan more effectively than music alone. As virtual reality technology improves, it may join headphones and MR compatible video goggles as an available distraction method.

Another helpful source of distraction for pediatric patients could be the patient's parent or parents. Having a parent involved with the scanning process may calm the patient and encourage him to cooperate; however, parental distress can further upset an anxious patient and complicate the scanning process [Alexander, 2012].

These techniques for educating the patient and helping the patient cope with the anxiety that can accompany an MRI scan all depend on the ability of the patient to understand instructions and communicate with the scan team. Due to the gap in communication abilities, these techniques are not useful for young patients such as neonates, infants, toddlers, and possibly elementary school aged children. Other patient populations, such as those with developmental delays and neurobehavioral disorders, may also have difficulty adhering to these protocols. Even in patients with developed and intact communication skills, the techniques outlined here do not actively prevent the patient from moving during the scan: they only help the patient feel more comfortable with the MRI environment.

3.4.3 Feed and Sleep Protocols

Neither sedation nor educational and behavioral techniques are appropriate to use with neonatal patients, but rs-fMRIs in neonates and infants are invaluable in studying early brain development and neurological diseases [Smyser and Neil, 2015]. A set of protocols have been developed specifically for scanning neonates without sedation. These protocols

are referred to as "feed and sleep" or "feed and bundle" protocols.

Windram et al. describe a protocol in which the infant is deprived of food for four hours prior to the scan [Windram et al., 2011]. At the scanning facility, the patient is fed by his mother, swaddled, and placed in a vacuum-bag immobilizer for the duration of the scan.

Rather than deprive the patient of food prior to the scan, Gale et al.'s protocol recommends timing the scan so that the patient is fed after arrival on site and less than 45 minutes before the scan [Gale et al., 2013]. The patient's ears are protected from the noise of the MR scanner by a layer of dental putty followed by headphones, and held in place by a hat. The patient is the swaddled and placed in the scanner once he is asleep. Additional foam padding is used to cushion the patient's head and provides extra noise protection.

Mathur et al. describe a protocol similar to the previous two: the patient's feeding schedule is adjusted so that he feeds 30-45 minutes before the scan time, and he is swaddled, given ear protection, and placed in a vacuum-bag immobilizer [Mathur et al., 2008].

When performed correctly, these protocols are generally successful and the neonatal patient will sleep for the duration of the MRI scan. However, the patient may shift slightly while asleep or may wake up and move mid-scan.

3.5 PROSPECTIVE MOTION CORRECTION

Since motion cannot be completely eliminated from rs-fMRI scans, different approaches have developed for correcting for the effects of motion after the scan. These approaches can be divided into two groups: those which monitor the patient's motion during the scan and those which work solely on the acquired sequences.

3.5.1 Optical Motion Correction

Several groups have developed methods for actively accounting for changes in the patient's position during an MRI scan. Optical-based methods record the patient's position using a combination of markers placed on the patient and one or more MR compatible optical

cameras placed the scanner bore. The changes in the patient position from one time point to the next are used to update the MR parameters in real-time. Real-time updates of the MR parameters result in decreased spatial and spin-history effects of motion in the acquired sequences.

The first report of successful prospective motion correction using optical cameras and markers was by Zaitsev et al. in 2006 [Zaitsev et al., 2006]. Their dual camera system was located outside of the MRI scanner and focused on the patient inside the system. Four reflective markers were attached to a modified mouthpiece originally designed for patient immobilization. Changes in the translation and rotation of the patient were recorded and processed during the exam. The processed changes were sent in real-time to the MRI scanner which used them to update the gradient orientations, RF frequencies, and RF phases at every time point during the acquisition process.

Aksoy et al. simplify this approach by using a single in-bore optical camera and replacing the 3D markers with a small 2D chessboard grid [Aksoy et al., 2008]. Properties intrinsic to the camera as well as information about the camera's placement within the MRI scanner were recorded prior as part of a calibration process. During the scan, patient movements recorded using the optical camera were used to calculate the relationship between the patient's position at the current time point in the physical space and the patient's position at the initial time point in the MR space. The transformation needed to translate between these two positions was calculated on a laptop and passed to the MRI scanner to correct for motion in real-time. The camera used to record the position of the chessboard is mounted on the head coil. If the patient moves his head significantly, the camera will only be able to record the position of part of the chessboard marker. This limitation makes it difficult for the computer vision processing to identify the independent features on the standard chessboard.

Forman et al. modified the chessboard marker to improve its flexibility [Forman et al., 2011]. To differentiate between the different blocks in the chessboard, they added a unique, machine readable symbol to each black block in the chessboard. The symbols were chosen to be unique even in the event of rotation so that the identification of each block would be robust to rotation movements. The chessboard marker was embedded with MR-detectable agar so that the position of the marker could be detected in the MRI scan as well as by the in-bore

camera. At each point during the scan, the image recorded by the in-bore camera was sent to a computer independent from the MRI controller. The independent computer detected the blocks of the chessboard and identified their spatial locations using the symbols contained within them. Their positions were checked by confirming the locations of the symbols with respect to each other. The confirmed locations of the corners of the black boxes were used to estimate the position of the patient, which was then sent to the MRI controller so that the magnetic gradients and RF hardware could be updated for the time point. The authors note that the latency of the system is a significant limitation to their system, but overall they experienced an increase in the accuracy of the estimates of the patient's position.

Several companies have developed commercial products for prospective motion correction in neurological images. KintetiCor's system uses a high resolution camera and a physical marker to detect motion [KinetiCor Biometric Intelligence, 2019]. The camera's resolution allows it to detect respiratory and cardiac motion through changes in skin displacement on the patient's forehead. The physical marker consists of pair of rectangles containing several concentric circles which are connected via a bridge across the nose. Any patient movement is reflected in the movement of the markers, which is also tracked through the camera. Both the camera system and the marker are MR compatible. Another company, TracInnovations, uses a stereo camera system to track all patient motion [TracInnovations, 2019]. At the start of the scan, the stereo camera obtains a point cloud of the patient's position at that time. The points in the point cloud are averaged together to create a primary marker. Small facial motions, cardiac motion, and respiratory motion, are monitored using the point cloud. Larger head motions are monitored using both the point cloud and the primary marker. These two systems both allow prospective motion correction to be turned on or off: if the prospective motion correction is off, the system will still acquire the motion parameters so that the motion can be corrected retrospectively.

The methods discussed above have a few limitations due to the optical camera setups. For precise real-time motion correction, the camera or cameras must be carefully placed so that the position of the marker on the patient can be recorded. They must have a clear line of sight, which means they will be in the same room as the MRI scanner, if not within the scanner bore. The cameras and markers must be MR compatible, and the positions of the

cameras and markers in physical space relative to the visual markers on the patient must be known. These positions are vital for the calculations used to measure the motions. Even if the motion measurements are accurate, the changes in position that are recorded and used to adapt the scan parameters will only be true for rigid body motion of the body part to which the markers are attached: any distortion of soft tissue will not be accurately accounted for during the motion correction unless the camera system was specifically built for and trained to do so.

3.5.2 External Sensors

Cameras are not the only type of external sensor that can be used to measure motion during a rs-fMRI scan.

There is a class of sensors which can take advantage of electrophysics properties of an MRI scanner. These sensors include wired nuclear magnetic resonance field probes, wireless inductivity coupled markers, and off-resonance markers. The fact that these sensors directly interact with the magnetic field of the MR scanner means that protocols using these sensors must be modified to account for them. As a result of the protocol modification, the scan time might need to be extended.

As mentioned earlier in this chapter, respiration is a source of patient motion. Since respiration is relatively periodic, it can be monitored and accounted for within a scan protocol via gating. Gating prevents an image from being acquired unless the patient is in the expected state. In the case of respiration, the expected state is either complete inhalation or exhalation. The state of a patient's respiration can be tracked using respiration bellows. After acquiring the MRI sequence, volumes in the sequence can be grouped depending on when they were recorded in the breathing cycle. By only using volumes recorded during the same stage of the breathing cycle, the effects of respiratory motion can be mitigated.

Ultimately, the addition of extra sensors complicate the process and set up of a rs-fMRI scan.

3.5.3 Image Space Motion Correction

Dosenbach et al. have developed a tool to evaluate motion in rs-fMRI sequences as they are acquired [Dosenbach et al., 2017]. It registers each frame to the initial frame of the rs-fMRI sequence immediately after the new frame is recorded. The parameters produced by this registration are used to calculate the framewise displacement between pairs of frames, which is then compared to a set of displacement thresholds associated with the scan quality. The number of frames that meet each threshold is used to determine how many more frames are needed to obtain five minutes of low-motion frames. This method for assessing the quality of a scan in real time is useful for ensuring images are acquired with a sufficient number of low-motion frames. It can also aid the technologists in determining whether to prematurely terminate a scan, which may be desirable if the amount of time needed to obtain enough low-motion frames is greater than the amount of time remaining for the patient in the scanner.

3.5.4 General Limitations of Prospective Motion Correction

All types of prospective motion correction introduce a delay into the scanning process. The delay is due to the additional processing of some metrics to determine the patient's position, the transmission of these metrics to the MR scanner, and the adjustments the scanner makes to its next set of measurements. These alterations to the image acquisition during prospective motion correction actively change the image as it is acquired. Maclaren et al. note that while prospective motion correction reduces imhomogeneities in the B_0 field, the B_0 field will still change when the patient moves and may change while the motion correction is occuring [Maclaren et al., 2013].

In order to view a scan not impacted by prospective motion correction, the patient often must undergo a second scan. It may be wise to build the second image acquisition into the same scan period as the prospectively motion corrected scan: unsuccessful prospective motion correction has the potential to drastically corrupt the acquired scan [Zaitsev et al., 2017].

Finally, though prospective motion correction has great power for managing motion during a scan, it cannot be used to recover motion-corrupted data in existing data sets.

3.6 RETROSPECTIVE MOTION CORRECTION

Many groups have put significant effort into developing techniques for motion correction after the scan is acquired. Here, we discuss several commonly used techniques: volume registration, denoising, and filtering.

3.6.1 Volume Registration

The rs-fMR image is stored in computer memory as a set of 3D matrices. The values in corresponding cells of each matrix are considered to be aligned in this digital space (voxel space). The voxel space is defined by the imaging protocol and relates to the physical space through the spatial resolution of the image. Even though the spatial and voxel spaces for the image align, the contents of the image volumes may be misaligned due to patient movement. Because we cannot assume that an image is completely motion-free, we cannot directly compare the contents of each image volume in the rs-fMRI sequence. However, we can use image registration to align the contents of the image volumes to reduce the impact of motion on patient position.

Image registration is the process of morphing the contents of one image so that they overlap optimally with another image. The morphing operations include translation, rotation, scaling, skewing, and nonlinear adjustments. The linear and affine operations in this list should be used to perform rigid body registrations for organs such as the brain. Nonlinear operations can be used to fine-tune the alignment of more pliable organs such as the liver. All morphing operations are applied to one image repeatedly until it's contents optimally match those of the static reference image as determined by a chosen similarity metric.

One of the earliest examples of image registration was described by Friston et al. in 1995 [Friston et al., 1995]. They performed image registration on positron emission tomography (PET) scans and MRI scans of a human brain. During the registration process, one scan was designated as the "reference" image, which remained stationary, and the other scan was designated as the "object" image, which was transformed to match the reference image. Constraining the alignment process to transforming a single image into the coordinates of

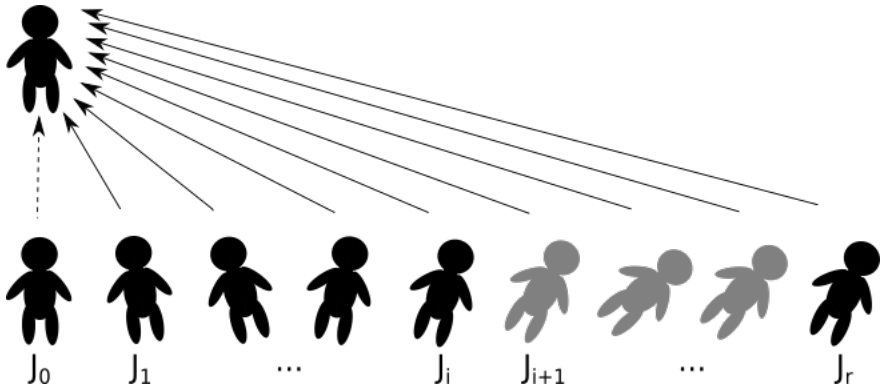

Figure 3: The traditional approach to volume registration in an rs-fMRI sequence consists of registering all volumes in the sequence to a single reference volume.

the other image rather than transforming both images into an independent coordinate frame simplifies the registration process.

When performing image registration on a sequence of image volumes, one volume must be chosen as the reference volume for the entire sequence. All other volumes in the sequence are registered to this volume. An example of this process can be seen in Figure 3. In subsequent work, Friston et al. used the first volume in the rs-fMRI sequence as the universal reference image [Friston et al., 1996]. Common choices for the reference volume include the volume with the least FD to all other volumes in the sequence, a volume produced by averaging all volumes in the sequence, or the first volume in the sequence [Friston et al., 1996] [Liao et al., 2005]. In our implementation, we chose to use the first volume in the sequence as the reference volume.

One drawback to this traditional approach to volume registration is that it only minimizes the differences between all the image volumes in the sequence and the reference volume. The key word here is minimizes: minimizing differences between image volumes does not mean that there are no differences between the image volumes. Image registration is an optimization problem, and its goal is to find the overlap between a pair of volumes with as few differences as possible either within a defined time period or until the optimization cost does not change above a certain tolerance for a certain amount of time. These practical

constraints on optimization problems mean that there may still be differences between other pairs of image volumes in the sequence that do not include the reference volume.

Variations on Friston et al.'s framework have been developed over the last two decades. Liao et al. suggested that a rs-fMRI sequence could be viewed as a hidden Markov model, and reflected this idea in their suggested registration framework [Liao et al., 2016]. They still use the first volume in the image sequence as the reference volume. Their framework uses the transformation of the previous volume to the reference volume to initialize the transformation for the current volume and the reference volume.

It has been demonstrated that image registration across the entire image sequence reduces the effects of motion on the image sequence, though they do note that motion also effects the image due to changes in the spin history of the image. These effects are not correctable by global volume registration alone and will be discussed later in this chapter.

3.6.2 Denoising

Denoising techniques can be applied to a rs-fMRI after global volume registration is completed. They consist of regressions of various confound variables.

Regression of the global signal (global signal regression, GSR) corrects for variance between temporal signals within a voxel and for the mean BOLD signal across all voxels [Power et al., 2014] [Satterthwaite et al., 2013] [Yan et al., 2013a] [Yan et al., 2013b]. GSR has been shown to reduce spuriously increased long-distance correlations in functional connectivity studies, but may inadvertently weaken shorter-distance connections [Jo et al., 2013] [Power et al., 2014] [Satterthwaite et al., 2012].

Other regression parameters which have been investigated include the six realignment parameters and their first-order derivatives [Power et al., 2012] [Satterthwaite et al., 2012] [van Dijk et al., 2012], realignment parameters from surrounding timpoints [Patriat et al., 2017] [Power et al., 2014] [Satterthwaite et al., 2013] [Yan et al., 2013b], signals from white matter or cerebral spinal fluid [Power et al., 2014] [Satterthwaite et al., 2013] [Yan et al., 2013b] [Jo et al., 2010], and components identified using principal or independent component analysis [Pruim et al., 2015] [Salimi-Khorshidi et al., 2014] [Behzadi et al., 2007]. Regression of

each of these sets of parameters has been shown to reduce the effects of motion in the sequence but not remove them entirely [Power et al., 2015] [Parkes et al., 2017].

3.6.3 Filtering

Filtering, which is also referred to as censoring, involves the identification and removal or interpolation of frames containing high quantities of motion. Two popular techniques are scrubbing and spike regression. Power et al.s scrubbing technique removes frames with more than 0.2 mm of FD [Power et al., 2012]. Spike regression identifies frames with large FD and replaces them with interpolated volumes [Satterthwaite et al., 2013]. Unfortunately, these filtering techniques ultimately result in the loss of data as frames are removed from the sequence. A third technique called despiking detects signal spikes at the voxel level and interpolates over the spikes [Jo et al., 2013] [Patel et al., 2014]. Despiking does not remove frames, but could accidentally remove valuable signals.

3.6.4 Spin History Distortion Correction

A number of post-acquisition methods have been developed specifically to correct for distortions due to the impact of motion on the magnetic field. The usability of these dynamic distortion correction methods has been studied in a few specific cases, but their generalizability has yet to be confirmed in a broader range of fMRI studies [Zaitsev et al., 2017].

3.7 IMAGE USABILITY

Even though the effects of motion on the patient position and the recorded signal can be measured, we still need gold standard criteria to determine whether an image containing motion can be used. Patients move slightly due to breathing and cardiac function, and the BOLD signal naturally fluctuates over time. Some motion is expected; however, we need to know how much motion can be present in the image before it is considered to be corrupted

by it. Power et al. established thresholds for FD and DVARS to determine the usability of a pair of images:

- FD less than or equal to 0.2 mm from previous volume, and
- DVARS less than or equal to 25 units on a normalized scale of [0, 1000] signal units [Power et al., 2014]

Image volumes that meet these criteria are considered to be low-motion. van Dijk et al. established that approximately five minutes of low-motion data is sufficient for use in functional connectivity analysis [van Dijk et al., 2012]. Unfortunately, it is often difficult to obtain enough low-motion data from patients to use in these analyses.

4.0 METHODS

4.1 MOTION CORRECTION

In the previous chapter, we discuss several techniques used to retrospectively correct motion. Motion correction pipelines may use denoising and filtering, but all pipelines begin with volume registration. In this section, we discuss a different approach to volume registration, how it compares to traditional volume registration, and how volume registration fits into a motion correction pipeline.

4.1.1 Directed Acyclic Graph Based Volume Registration

As discussed previously, the major drawback to Friston et al.'s approach to volume registration is that it only minimized the positional differences between the reference volume and the rest of the sequence. This drawback demonstrates an inability for the traditional approach to account for relationships in the patient's position throughout the scan. Intuitively, we know that the patient's position at any volume in the scan is more similar to his position in the immediately previous or subsequent volume than to another randomly chosen volume in the image.

In our proposed framework, we wish to account for these spatiotemporal relationships between temporally neighboring volumes in the sequence. To accomplish this goal, we start by viewing the rs-fMRI sequence as a directed acyclic graph (DAG). A DAG consists of a set of nodes and edges. Each edge has a direction associated with it and connects a pair of nodes. Since a DAG contains no cycles, there is no possible path back to a node once it has been traversed.

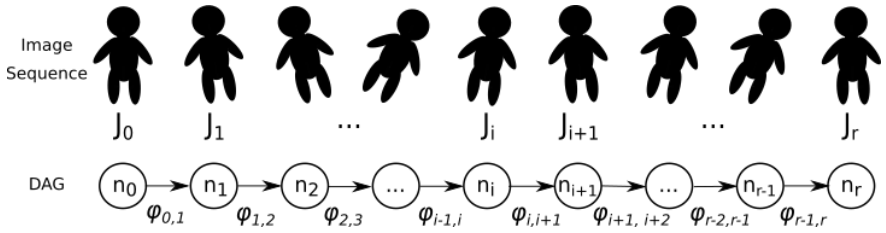

Figure 4: A rs-fMRI can be viewed as a directed acyclic graph where each volume is a node and the edges connect from each volume i to the following volume $i+1$.

In the case of an rs-fMRI, each volume can be considered a node. The relationship between each pair of temporally neighboring volumes is represented as a directed edge connecting the node for the first volume to the node for the next volume. The acyclic nature of the DAG means that once a patient was in a specific position, he will never return to that exact same position with the exact same neurons firing. The position of the subject and his brain activity as measured by the BOLD signal may be similar in subsequent image volumes, but it will never be precisely the same. The perspectives of an rs-fMRI sequence as a set of images and of the sequence as a DAG can be seen in Figure 4.

The cost of transitioning from one node to the next in our DAG has a parallel representation to the combination of the positional transformation needed to align volume i to volume $i+1$ and the signal change between the volumes. This representation can be written as

$$J_{i+1} = \phi_{i,i+1} J_i + \delta s_{i,i+1} + \epsilon \tag{4.1}$$

where J_i and J_{i+1} are volumes i and $i+1$, $\phi_{i,i+1}$ is a matrix of transformation parameters that must be applied to J_i to achieve the patients position in J_{i+1}, $\delta s_{i,i+1}$ is the natural change in BOLD signal, and ϵ is the change in BOLD signal due to motion. Currently, there is no way to estimate the natural change in BOLD signal and the change in BOLD signal due to motion without incorporating additional information about the MRI scanner and the patient that is not included in a rs-fMRI. We simplify our representation of the relationship

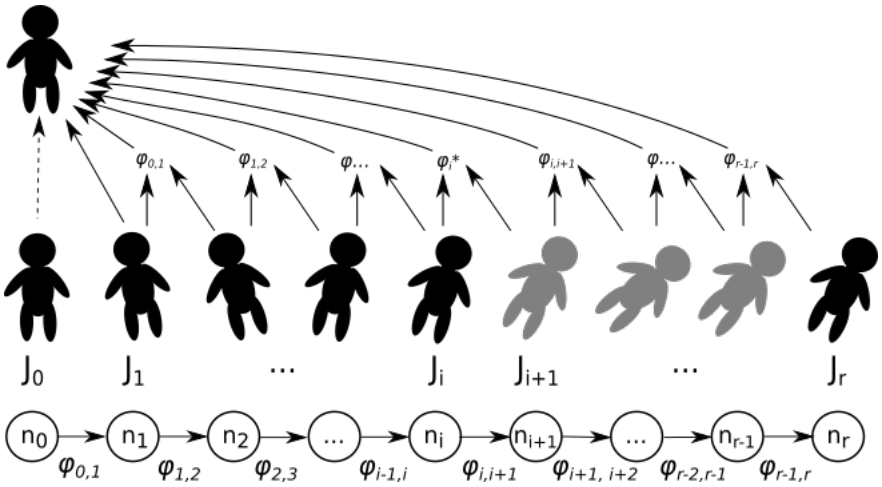

Figure 5: The traditional approach to volume registration in an rs-fMRI sequence consists of registering all volumes in the sequence to a single reference volume.

between two volumes to

$$J_{i+1} = \phi_{i,i+1} J_i + \epsilon^* \tag{4.2}$$

where ϵ^* is the change in the BOLD signal that cannot be accounted for after aligning the patients position in the two volumes. Here, we use the notation ϵ^* to represent the generic error change in BOLD signal across any pair of volumes.

After aligning two volumes i and $i+1$, we will then align volumes $i+1$ and $i+2$:

$$\begin{aligned} J_{i+2} &= \phi_{i+1,i+2} J_{i+1} + \epsilon^* \\ &= \phi_{i+1,i+2}(\phi_{i,i+1} J_i + \epsilon^*) + \epsilon^* \\ &= \phi_{i+1,i+2}\phi_{i,i+1} J_i + \epsilon^{*'} \end{aligned} \tag{4.3}$$

Traditional volume registration assumes that

$$\phi_{i,i+2} = \phi_{i+1,i+2}\phi_{i,i+1} \tag{4.4}$$

and calculates $\phi_{i,i+2}$ directly. We argue that this assumption is not true in all cases. Rather than directly calculate $\phi_{0,i}$ and use it to align volume i to the reference volume as the traditional method does, we calculate each component ϕ that is a factor of $\phi_{0,i}$. Each component $\phi_{i,i+1}$ is combined with the preceding $\phi_{0,i}$s to recursively align volume $i+1$ to the reference volume without making the large and often inaccurate transformations required by directly calculating $\phi_{0,i+1}$. This process is outlined in Figure 5.

4.1.2 Motion Correction Pipeline

After performing volume registration to ensure the patient is in the same physical space throughout the image sequence, the image sequence may still contain artifacts due to motion. Many pipelines exist for correcting motion in registered rs-fMRIs.

4.2 MOTION METRICS

In the previous chapter, the gold standard thresholds for rs-fMRI usability were discussed. These thresholds use the FD and DVARs metrics between neighboring volumes. While the FD and DVARs metrics quantify the volume-to-volume motion well, they do not quantify the overall motion contained in the image sequence. Other metrics, such as the Dice coefficient and the correlation ratio, may be useful in quantifying whole-sequence motion.

4.2.1 Dice Coefficient

The Dice coefficient was proposed by Lee R. Dice in 1945 [Dice, 1945]. Dice examined several existing metrics for measuring association, and finding them lacking, proposed his own "coincidence index". His coincidence index measures the association between a number of samples a where condition A is true and a number of samples b where condition B is true:

$$Index = \frac{2h}{a+b} \tag{4.5}$$

In this equation, h represents the number of samples where both conditions A and B are true. His index can take on any value between 1.0 and 0.0 such that a value of 1.0 means that conditions A and B are true for all samples. Similarly, a value of 0.0 means that conditions A and B are never both true for any sample. While this index is a count of samples that meant both conditions and not a true probability, Dice suggests that the chi-squared test can be used to determine if the combinations of conditions in the samples from a set of data is meaningful or due to random chance.

Many medical imaging researchers have adapted the Dice coefficient to measure the overlap between pairs of images. Zijdenbos et al. trained an artificial neural network to semiautomatically segment brain MRIs and compared the generated segmentations to manual segmentations using the Dice coefficient [Zijdenbos et al., 1994]. Zou et al. used the Dice similarity coefficient in their analysis of the reproducibility of manually segmented MRIs and the accuracy of automatic segmentations of the same images for prostate and brain tumor datasets [Zou et al., 2004]. Liao et al. used it to measure the accuracy of a volume registration framework for aligning manual segmentations of multiple organs in fetal images [Liao et al., 2016]. Bharatha et al. performed a study on pre- and intra-operative images of the prostate. They segmented the images, generated deformable finite element models of the segmentations, and used the Dice coefficient to compare the registered segmentations and finite element models [Bharatha et al., 2001].

It should be noted that the Dice coefficient as used in these contexts is a measure of similarity of items from two categories which take on binary conditions. Additionally, all studies mentioned in the previous paragraph require a manually segmented gold standard image to which the automatic segmentations or registered images can be compared. Medical images do not naturally have binary values, nor is it always reasonable to obtain manual segmentations of all images in a dataset. In cases where a good image segmentation cannot be obtained, other similarity metrics such as mutual information and cross correlation should be used instead.

4.2.2 Correlation Ratio Matrix

The correlation ratio is an asymmetrical, spatially informed measure of the overlap between images. It is different from other similarity metrices in that a lower correlation ratio indicates a better alignment between two images rather than a worse alginment.

The earliest symbolic representation of the correlation ratio is

$$\eta = \frac{\Sigma}{\sigma_y} = \frac{\sqrt{\frac{\sum(n_x(\overline{y}_x - \overline{y})^2)}{N}}}{\sigma_y} \tag{4.6}$$

where n_x is the number of samples in any one set x, $\overline{y}_x$ is the average of the samples in x, $\overline{y}$ is the average of all samples in all sets, σ_y is the standard deviation of all samples in all sets, and N is the total number of samples across all sets [Rugg, 1917]. The meaning of this equation was simplified by Ayres, who describes it as "the ratio between two standard deviations" [Ayres, 1920]. In Equation 4.6, the numerator is the standard deviation of a single set of samples with respect to all sets of samples, and the denominator is the standard deviation of all sets of samples. The process of calculating the individual components of this equation are outlined in [Rugg, 1917].

The correlation ratio was proposed for use in medical imaging applications in 1998 and compared to other similarity metrics. Roche et al. provide an example of algining two black images, one with a uniform gray stripe and the other with a horizontal gray gradient, such that the overlap between the two images is maximally similar [Roche et al., 1998a], [Roche et al., 1998b]. They show that the mutual information metric has a maximum value at every translation of an integer number of pixels while the correlation ratio had a maximum value at one single alignment. They apply the correlation ratio to MR images as well as computed tomography and positron emission tomography images. Their experiments suggest that in the context of multimodal registration, the correlation ratio balances accuracy and robustness.

In the context of medical imaging, the correlation ratio measures the functional dependence between a pair of images X and Y. The correlation ratio of Y given X is

$$\eta(Y|X) = \frac{Var[E(Y|X)]}{Var(Y)} \tag{4.7}$$

This equation is comparing the energy of Y in X to the total energy of Y. If X and Y overlap in area Ω, the number of pixels in that area is $N = Card(\Omega)$. Since X is known, it can be divided into sets of pixels Ω_i where each set is comprised of locations in Ω where the pixels X have the same value i.

Because the correlation ratio shows is a strong metric for measuring the similarity between two images, we suggest using it to quantify the similarity between all volumes in an image sequence. We choose to refer to this metric as the correlation ratio matrix. For a sequence of length l, the correlation ratio matrix M is a square, asymmetrical matrix of size $l * l$. Each cell in M is calculated as

$$M_{i,j} = \eta(J_i, J_j) = \frac{Var[E(J_i|J_j)]}{Var(J_i)} = \frac{\sqrt{\frac{\sum |J_i|(\overline{J_i} - \overline{J_i \cap J_j})^2)}{|J_i \cap J_j|}}}{\sigma_{J_i \cap J_j}} \tag{4.8}$$

where J_i and J_j are volumes $i \in l$ and $j \in l$ in the sequence, respectively, $|*|$ indicates the number of voxels in the operand, $\overline{*}$ indicates the average of the voxel values in the operand, and $J_i \cap J_j$ is the volume of space where images J_i and J_j intersect.

Since the matrix M is quite large, using statistics describing M rather than M itself can simplify analyses. On the other hand, the whole matrix M may be more comprehensively analyzed using statistical tests such as the t-test.

4.3 ANALYSIS OF MOTION CORRECTION

The purpose of motion correction is to remove noise from valuable signal in an image. The amount of motion removed from an image can be quantified using the FD and DVARS usability thresholds, but that analysis does not explain how volume registration and motion correction techniques generalize to larger populations.

Statistical analyses can be used to identify general trends within a data set. Statistical tests can be used to compare images before and after motion correction within each subject population. They can also indicate the degree of significance of the effects of volume registration and motion correction.

4.4 MOTION PATTERNS

We suggest that the ways that patients move are specific to certain patient groups. For example, fetal patients live suspended in amneotic fluid and as such are subject to different physical constraints than patients in other age groups. Neonatal patients are often scanned using a "feed and bundle" protocol, which often results in them sleeping through the scan. However, neonatal patients sometimes wake up during the scan. The way a baby woken up from a nap moves is different from how a fidgety preadolescent moves, though the terminology to define how these movement patterns differ is somewhat lacking.

There is also a chance that patients within the same age group move differently possibly due to their cognitive state. Preadolescents who have ADHD likely become bored and fidgety in the MR scanner at different rates then their non-ADHD counterparts. Adults suffering from dementia may have more difficulty remaining still for the duration of a scan than adults with similar demographics and no dementia.

These patterns are essentially signals specific to different categories of patients. Machine learning techniques are useful for identifying patterns in signals from different sources. Unsupervised learning techniques group samples from a population based on the patterns in their features. The results of unsupervised clustering algorithms can be visualized and analyzed to determine how the computer chose each group of samples.

Another approach to analyzing these signals is regression. Regression models the relationships between a set of independent features and an outcome or set of outcomes. For example, the linear regression could be used to evaluate the relationship between motion metrics and the severity of neurodevelopmental outcomes or patient age.

In addition to machine learning and regression, other techniques from the biomedical imaging and computer vision domains may be used. Supervised machine learning models may also be trained to predict a clinical or behavioral outcome based on a patient's image features.

4.5 IMPLEMENTATION: TOOLS AND LIBRARIES

The registration frameworks described in this section were implemented in Python using the nipype (Neuroimaging in Python Pipelines and Interfaces) library [Gorgolewski et al., 2011]. Affine volume registration was performed using ANTs (Advanced Normalization Tools) [Avants et al., 2014]. The metric used to estimate the dissimilarity between the pairs of volumes being registered was cross-correlation with a local window size of 5 voxels.

To calculate metrics, we used several existing tools. FLIRT (FMRIBs Linear Image Registration Tool) was used to calculate the correlation ratio between each possible pair of volumes in the sequences [Jenkinson and Smith, 2001] [Jenkinson et al., 2002]. We then used the average and standard deviation of the correlation ratio distribution of each image to compare the images. We calculated the FD and DVARS metrics defined by Power et al. using the FSLMotionOutliers tool [Power et al., 2012]. These metrics were calculated for each image and were used for evaluation of the efficacy of the registration frameworks.

5.0 DATA

The data used to test the hypothesis and aims introduced in the previous chapter are drawn from several subject populations. Because motion causes problems in MR images across all stages of life, we used images from cohorts of healthy and CHD fetal, neonatal, preadolescent, and adult subjects gathered in as part of ongoing studies. Data from these studies was obtained through studies approved by the IRB at the Children's Hospital of Pittsburgh of UPMC and the University of Pittsburgh. The data is stored and accessed in compliance with all HIPPA policies.

We use data from a simulated phantom as well as healthy adult human phantoms. The healthy adult human phantom data collection was also approved by the IRB at the Children's Hospital of Pittsburgh of UPMC and the University of Pittsburgh and is stored and accessed in compliance with all HIPPA policies.

The final data set we use is from the Alzheimer's Disease Neuroimaging Initiative (ADNI) database (adni.loni.usc.edu). The ADNI was launched in 2003 as a public-private partnership, led by Principal Investigator Michael W. Weiner, MD. The primary goal of ADNI has been to test whether serial magnetic resonance imaging (MRI), positron emission tomography (PET), other biological markers, and clinical and neuropsychological assessment can be combined to measure the progression of mild cognitive impairment (MCI) and early Alzheimer's disease (AD). For up-to-date information, see www.adni-info.org.

5.1 NEONATAL SUBJECT POPULATION AND IMAGES

Neonatal subjects are recruited as part of a prospective observational study. The subjects were scanned using a 3T Skyra (Siemans AG, Erlangen, Germany). They were unsedated during the scans and a "feed and bundle" protocol was used to prevent motion during the scans [Windram et al., 2011]. The newborns were positioned in the coil to minimize head tilting. Newborns were fitted with earplugs (Quiet Earplugs; Sperian Hearing Protection, San Diego, CA) and neonatal ear muffs (MiniMuffs; Natus, San Carlos, CA). An MR-compatible vital signs monitoring system (Veris, MEDRAD, Inc. Indianola, PA) was used to monitor neonatal vital signs. All scans were performed using a multi-channel head coil. The parameters for the resting-state BOLD MR scans were FOV=240 mm and TE/TR=32/2020 ms with interplane resolution of 4x4 mm, slice thickness of 4 mm, and 4 mm space between slices. The acquired images contained 150 volumes where each volume consisted of 64x64x32 voxels^3.

5.2 PREADOLESCENT SUBJECT POPULATION AND IMAGES

As part of a multicenter study of CHD in preadolescents, we collected rs-fMRIs from nine sites throughout the United States. These images were of patients in the age range of 9 to 13 years who either had CHD or were healthy with no neurocognitive impairments. In addition to the MRI scans, subjects who participated in this study were asked to participate in additional testing either to determine their neurocognitive outcome status or to perform genetic analyses.

5.3 ADULT SUBJECT POPULATION AND IMAGES

As the prognosis for patients with CHD improves, their life expectancy also increases. The aging CHD population presents new questions about the connection between CHD and

neurocognitive challenges associated with aging. As patients age, there is an expectation that their images will contain less motion for a time. If a patient begins to show signs of cognitive impairment due to aging, it can be expected that their images will begin to contain more motion as their neurocognitive state deteriorates.

We include a cohort of adult subjects over a wide range of ages in our study. The purpose of using images from this cohort is to demonstrate the generalizability of the DAG-based framework to adult patients as well as its use in different clinical populations. This cohort is being studied as part of an ongoing, prospective study of CHD and neurodevelopment. The data collected for these subject includes rs-fMRIs, behavioral, and clinical data from healthy and CHD adult subjects.

5.4 FETAL SUBJECT POPULATION AND IMAGES

Fetal subjects have different constraints on their physical environment than neonates, preadolescents, and adults. As a result, they exhibit unique patterns of motion. The previous subject cohorts discussed in this chapter have the following commonalities: the subject experiences the full effects of gravity, the subject is lying on his back in an MRI scanner, and the subject's head motion is limited by the head coil within the MRI. Any motion in these images is a direct result of the subject himself moving, whether passively (cardiac motion and breathing) or actively (fidgeting or looking around).

A fetal subject is scanned in vivo. He is suspended in amniotic fluid within his mother. The amniotic fluid has buoyancy that reduces the effects of gravity and allows a fetal subject significant freedom of movement. The fetus can rotate, shift, and flip in ways that can only be accomplished when floating in a body of water. The properties of the uterus constrain the physical space in which a motion could occur, but not as much as the head coil and gravity do to the other patient cohorts. A fetus is not guaranteed to be in any specific position at the start of the scan: the scan begins when the mother is ready, not when the fetus achieves a certain pose.

The fetal subjects underwent fetal echocardiography scans in a cardiac clinic to determine

whether they were healthy or had a form of CHD. They were then scanned on an MRI scanner. Images of the fetal brain and the placenta were acquired for each subject.

We are interested in both the fetal brain and placental images for our work because of the relationship between placenta and brain development. However, these organs have very different physical properties. The fetal brain is a rigid structure floating and moving within the amneotic fluid. It undergoes translation and rotation as a single unit due to passive and active maternal and fetal motions. The placenta, on the other hand, is anchored in place on the uterine wall. It may undergo small translations or rotations due to maternal motion, but it will respond differently to fetal motion. Fetal motions cause nonlinear deformations of the pliable placenta that can only be adequately accounted for using nonlinear registration algorithms. Nonlinear registrations have the potential to deform brain images into physically impossible shapes, so the fetal brain and placenta were manually segmented in their respective images so that each organ could undergo independent motion correction.

The segmenters were one of a group of four researchers. While one researcher trained the other three group members, the interrater agreement between them is still being determined.

5.5 SIMULATED PHANTOM IMAGES

Every MRI scanner is different, so a stand-in model for an organ or tissue type is often used to calibrate an MRI scanner. The model is designed to have specific physical properties which mimic the physical properties of the organ or tissue. These properties can be accurately measured during the design process of this model so that the radiologist or researcher looking at images of the model can know the ground truth of the model. Because these models mimic true organs and tissues, they are called phantoms.

We will generate a simulated phantom image using the rs-fMRI of a healthy adult male. A single volume will be selected from the rs-fMRI sequence. This volume will be duplicated to create a generated image with 150 instances of the same volume. This sequence will be our base phantom sequence.

A copy of the base phantom sequence will be made and a subvolume in the same location

of every volume will be selected. In the subvolume of each frame, a small amount of noise generated using a normal Gaussian distribution will be added to simulate changes in blood oxygen level-dependent signal over time. The noise will be generated from a normal Gaussian distribution will be added to each frame. This image sequence will be referred to as our BOLD phantom sequence.

5.6 HUMAN PHANTOM IMAGES

One of the major challenges in the medical imaging field is collecting a large enough set of data with a high enough quality to generate statistically significant results. As part of a multisite study, a set of five healthy adult male subjects were scanned at several different sites within a period of ten weeks.

These subjects are considered human phantoms because of their health adult status, but they still may contain some motion. Their images are included in this study so that we can determine the consistency and effects of the motion correction pipeline on images of the same subject across time.

6.0 AIMS

6.1 VOLUME REGISTRATION IN A MOTION CORRECTION PIPELINE

All images in each data set and cohort underwent both types of registration independently. The registered and original images are compared to the Power et. al. usability thresholds. The results at this stage answer the question of whether or not the DAG-based registration technique is more effective than the traditional registration technique for reducing motion in the initial step of a motion correction pipeline.

Next, each pair of registered images will undergo a motion correction via an independent component analysis (ICA) pipeline outlined by Beckmann and Smith and implemented as FMRIB's MELODIC tool [Beckmann and Smith, 2004]. The results of this experiment show how the DAG-based framework fits into an existing, comprehensive motion correction pipeline.

6.1.1 Simulated Phantom

The phantom experiments will be used to probe the volume registration technique. By applying the DAG-based and traditional registration techniques to the base phantom sequence, we will be able to evaluate the degrees of positional and signal change errors each technique may introduce into the registration process. After determining the baseline error, we will apply both registration techniques to the BOLD phantom sequence. The registered versions of the BOLD phantom sequence will be compared to each other and to the original BOLD phantom sequence to determine how well each registration retains the BOLD signal.

This particular experiment will be one of the first to investigate how much true BOLD

signal is preserved through motion correction. One of the major drawbacks to existing motion correction pipelines is that they remove signal along with noise. In clinical data, there is no way to know the ground truth signal contained within the image; however, simulated phantom images have a de facto known ground truth signal. The design for this experiment can be used to evaluate how much BOLD signal is recovered by other motion correction pipelines, and how close the recovered signal is to the signal of interest.

6.1.2 Human Phantom

The human phantom images from all sites will be used both as a set of true healthy control adults and as examples of low motion images of the same subjects taken at multiple sites.

6.1.3 Clinical Images

Neonatal Cohort. Our set of neonatal subjects includes a cohort of 74 healthy neonates. Each subject in this cohort underwent an MRI scan, and the rs-fMRIs obtained during this process were compared to Power et al.'s positional and signal change usability thresholds. Of the 74 subjects, 17 of them had rs-fMRIs which did not meet the usability criteria. These high motion images were used to test the feasibility of the DAG-based volume registration framework.

These images were ideal for the feasibility study for three reasons. First, the neonates were healthy, which eliminates disease status as a confounding variable in the analysis of the registered images. Second, the neonates in this study were scanned using a feed and sleep protocol. Because the neonates were asleep during the scan, they generally did not move very much. The high-motion neonates are an obvious exception to this concept, but many of the high-motion images contained long periods where the subject was stationary. Evaluating the DAG-based framework on data with various patterns of motion and different periods of low and high motion allowed us to explore the effects of the DAG-based algorithm in different combinations of motion features. Third, these images were too corrupted by motion to be used in other analyses. Applying both the DAG-based framework and the traditional registration framework to these images provided the opportunity to compare the

performances of both registration frameworks to each other in the context of the usability gold standard thresholds.

Preadolescent Cohort. The multicenter imaging study of preadolescent subjects provides a unique opportunity to evaluate the efficacy of the DAG-based framework on a large subject cohort containing variable amounts of motion. The outcome of this experiment will be used in the next experiment to determine if there are any site-specific or vendor-specific variables influencing patient motion.

Adult Cohorts. The adult cohorts encompass many clinical outcomes and a wider age range than the other clinical populations.

Fetal Cohort. As the fetal subjects have both neurological and placental images, their data will be used to examine the impact of volume registration on different organ types.

6.2 DESCRIBING MOTION PATTERNS

In previous sections we describe practical knowledge about how fetal, neonatal, preadolescent, and adult patients move in different ways during MRI scans. We wish to quantify these movement patterns using the metrics described in Chapter 4 and identify appropriate terminology that can be used to describe them.

6.3 IDENTIFYING MOTION PATTERNS

Machine learning techniques can be used to classify images as belonging to different groups, but many of these techniques use difficult to interpret "black box" logic. In some cases, examining the logic behind a classification reveals patterns in a dataset which a human missed but a computer detected. These patterns can be helpful for improving human classification of the images, but they may also be based on artifacts which were not filtered out during preprocessing.

6.3.1 Demographic-Related Motion Patterns

To ensure that there are no confounding signals in our datasets, we first use unsupervised machine learning techniques to identify correlations between subject images and their demographic data. The techniques we will use are several types of clustering (agglomerative, k-means, and spectral) as well as principle component analysis (PCA) and regression. Features of the images before and after registration will be used as training data for each model and different demographic features will be used as the true classes.

Phantom Images. The phantom images are included in this analysis, though no significant results are expected other than potential site specific results.

Clinical Cohorts. Any demographic features which influence the division of patients into groups will be reported and accounted for during later analyses. After identifying and accounting for demographic groups, we will expand the analysis to clinical and behavioral outcomes.

6.3.2 Clinical-Related Motion Patterns

In addition to evaluating the effects of the DAG-based framework within the context of a motion correction pipeline, the registered images are used to explore the relationship between motion and clinical outcomes. Unsupervised machine learning techniques such as agglomerative clustering and k-means clustering are applied to the data. The results of the clustering techniques elucidate whether there are patterns in motion specific to certain patient groups. These groups could include patients with similar clinical outcomes, patients from the same site, or potentially other clinical or demographic groups.

7.0 PRELIMINARY RESULTS

7.1 COMPARISON OF VOLUME REGISTRATION METHODS

7.1.1 Subject Position Variability in the Registered Images

Each rs-fMRI sequence in the cohort underwent registration using both frameworks. For each sequence, the correlation ratio between every possible pair of volumes was calculated. A set of metrics of the correlation ratio matrices for each sequence can be seen in Table 1. This table shows that the original sequences generally have higher average correlation ratios and contain more variation in their correlation ratios than the globally registered images. The registration methods were able to reduce the mean and variability of the correlation ratios across all subjects in the cohort who had original correlation ratio averages of at least 0.035.

7.1.2 Comparison of Motion Correction Methods

The FD and DVARS values were calculated to determine how many volumes in each registered sequence met the FD and DVARS thresholds. The FD and DVARS values also considered to be distribution functions representing the effects of no registration, traditional registration, and DAG-based registration. These distributions were compared using the Kolmogorov-Smirnov test, which compares the empirical distribution functions of two samples. There were statistically significant differences between the FD and DVARS values of all sequences at $p < 2.2E - 16$. Statistics calculated for the FD and DVARS value histograms of both motion correction methods can be seen in Table 2.

Power et al.s usability thresholds were used to determine how many volumes were recov-

ered by each framework [Power et al., 2014]. Table 3 shows the number of volumes meeting each threshold, with the traditional and DAG-based frameworks recovering 2% and 10% of volumes, respectively. These results show that the DAG-based registration technique produces sequences with lower FD and DVARS value than the traditional global registration method does.

Table 1: The mean and standard deviation for each sequences correlation ratio matrix for every subject.

	Original Sequence		**Traditional Registration**		**DAG-based Registration**	
Subject	**Mean**	**Standard Deviation**	**Mean**	**Standard Deviation**	**Mean**	**Standard Deviation**
0	0.04476	0.02707	0.03842	0.01167	0.03194	0.01082
1	0.04339	0.02926	0.03323	0.00771	0.03903	0.01315
2	0.03464	0.01773	0.04522	0.01359	0.03768	0.00775
3	0.03431	0.00264	0.03203	0.01097	0.03528	0.00289
4	0.03288	0.00462	0.02601	0.00981	0.03364	0.00514
5	0.03234	0.01376	0.02986	0.00958	0.03390	0.00800
6	0.03145	0.00730	0.02691	0.00685	0.03065	0.00496
7	0.02970	0.03314	0.03331	0.00736	0.03025	0.00969
8	0.02728	0.01044	0.03060	0.00500	0.03359	0.00791
9	0.02467	0.00305	0.03354	0.00513	0.02467	0.00303
10	0.02446	0.00163	0.03535	0.00293	0.02446	0.00163
11	0.02422	0.01161	0.02958	0.00559	0.02617	0.00981
12	0.02338	0.00060	0.02467	0.00304	0.02338	0.00060
13	0.02280	0.00101	0.02447	0.00163	0.02279	0.00101
14	0.01968	0.01040	0.02338	0.00060	0.02740	0.00664
15	0.01942	0.00526	0.02279	0.00101	0.02939	0.00548
16	0.01414	0.00133	0.01512	0.00178	0.01520	0.00184

Table 2: The mean, median, standard deviation, skewness, and kurtosis of the histograms of FD and DVARS values for all image types were calculated. The histograms for the DAG-based method have lower means, medians, and standard deviations than those of the first volume correction method.

	FD Values (mm)			**DVARS Values (units)**		
Statistic	**None**	**Traditional**	**DAG-based**	**None**	**Traditional**	**DAG-based**
Mean	1.07	2.18	1.22	63.14	135.15	97.23
Median	0.30	1.46	0.56	35.19	133.48	77.75
Standard Deviation	1.97	2.35	1.61	70.00	83.48	77.14
Skewness (-)	3.86	3.08	3.00	2.76	1.13	1.55
Kurtosis (-)	23.29	17.74	17.12	14.28	7.79	7.44

Table 3: The number of frames recovered by each global volume registration framework for each threshold.

Threshold	**None**	**Traditional**	**DAG-based**
FD (0.2 mm)	966	175	569
DVARS (25 units)	781	78	297
Both	619	61	258
Both (%)	24.27%	2.39%	10.11%

8.0 DISCUSSION

8.1 COMPARISON OF VOLUME REGISTRATION METHODS

Resting-state BOLD MR images are used to evaluate the functional architecture of a patients brain . Because resting-state BOLD images are highly susceptible to motion, development of strong post-acquisition motion correction techniques is vital. Current pipelines for mitigating motion after sequence acquisition vary in terms of efficacy and effectiveness, but all begin with global volume registration. In this study, we compared the corrective performance of two global volume registration methods, the traditional framework and a novel DAG-based framework, on a set of 17 neonatal rs-fMRIs.

The correlation ratio matrices, FD, and DVARS values were calculated for each sequence. The decrease in the mean and standard deviations of the correlation ratio matrices for the registered sequences indicate that global volume registration reduces some effects of motion in rs-fMRIs. The histograms of the FD and DVARS values in the registered sequences show that the DAG-based method was better able to correct volumes to meet Power et als thresholds than the traditional registration method. These results indicate that the DAG-based global registration method is better able to reduce the effects of motion than the traditional global registration method when correcting motion in neonatal images. While no entire sequences were recovered, some high-motion volumes within each sequence were recovered by the DAG-based registration method that were not recovered by the traditional registration method.

8.1.1 Relation to Existing Work

To the best of our knowledge, the only other study that has used a variant of the DAG-based method was performed by Liao et al [Liao et al., 2016]. Liao et als dataset consisted of 10 fetal rs-fMRIs. In each of these sequences, the fetal brain, fetal liver, and placenta were manually segmented in the first volume of the sequence as well as in five other randomly chosen volumes. These overlap of these manual segmentations before and after registration as measured using the Dice coefficient was used to quantify the amount of motion in each sequence. Even though the Dice coefficients increase more in each sequence after Liao et al.s registration than after traditional registration, their measure of positional change fails to quantify any changes in position between any other pairs of volumes that do not have manual segmentations.

8.1.2 Limitations and Future Work

Subject motion during rs-MRI scans affects both the recorded position and orientation of the subject as well as the established magnetic spin gradients within the skull. The DAG-based technique can correct the positional effects of motion, but it cannot correct the effects of the motion that disrupt the magnetic spin gradients. Methods for prospectively estimating subject motion exist and can be used to change slice positions in each volume during acquisition. Retrospective techniques to correct for this effect will require shot-to-shot modeling of macroscopic B_0 fields and are beyond the scope of the present research.

In the future, we plan to apply the DAG-based technique to a cohort of preadolescent images for the purpose of characterizing motion in a large cohort as well as to a cohort of neonatal images to address the problem of correcting motion of multiple organs in images with large amounts of motion.

8.1.3 Conclusions

In this feasibility study, we applied two global registration methods to set of rs-fMRIs of 17 healthy neonates. We showed that both global registration techniques reduce the amount

of motion in the images as measured using the correlation ratio. We then showed that the DAG-based framework is better at correcting images to a pair of established gold standard thresholds for resting-state BOLD MRI usability than the traditional framework. In the future we plan to apply the DAG-based framework to other patient populations and multi-organ problems.

APPENDIX A

POTENTIAL PUBLICATION TOPICS

- DAG-based Volume Registration for Recovering Neonatal rs-fMRIs: present DAG-based volume registration in the context of a small, healthy cohort; feasibility study. ***Note: paper being revised for resubmission to JAMIA.***
- DAG-based Volume Registration in a Comprehensive Motion Correction Pipeline for CHD and Healthy Patients: generalize the results of the previous paper to more age groups, motion types, and clinical outcomes.
- Does Motion Correction Recover Signal: Discuss the simulated phantom images and how both registration methods and the motion correction pipeline affect them.
- Analysis of Human Phantom rs-fMRIs for a Multicenter Neuroimaging Study
- Patterns of Motion Across Life: describe the different motion patterns seen in different age groups; propose a formal scale of motion in terms of frequency, severity, and entropy.
- Relationships between motion metrics and clinical, behavioral, and demographic data among different CHD and healthy patient populations.

Other publications could be any combination of age groups, clinical status, and neurological conditions at different stages of analysis pipeline including volume registration, motion correction, and functional connectivity analysis.

APPENDIX B

PROPOSED TIMELINE

Month	**Objectives**
June 2019	Begin coordinating with lab members to find data for all subjects from all cohorts. Generate simulated phantom images. Determine organization system for images and clinical data for each cohort. Determine organization system for registered images and results.
July 2019	Continue obtaining and organizing data, if needed. Run both volume registrations and the motion correction on preadolescent cohort Structure analysis of volume registration analyses. Submit volume registration feasibility paper.
August 2019	Analyze corrected preadolescent images. Run volume registrations and the motion correction pipeline on the whole neonatal cohort. Outline preadolescent motion correction paper.

Month	Objectives
September 2019	Analyze corrected neonatal images. Run volume registrations and the motion correction pipeline on the fetal images. Write preadolescent motion correction paper.
October 2019	***Update on project status to committee.** Run volume registrations and the motion correction pipeline on the ADNI images. Analyze corrected fetal images. Begin unsupervised machine learning to identify patterns of motion in fetal, neonatal, and preadolescent images.
November 2019	Run volume registrations and the motion correction pipeline on the phantom images. Run volume registrations and the motion correction pipeline on the adult CHD images. Continue identifying patterns of motion in fetal, neonatal, and preadolescent images. Also incorporate adult images.
December 2019	Analyze corrected phantom and adult CHD images. Outline paper on age-based patterns of motion, descriptions of motion, and quantification of motion. Identify clinically valuable outcomes to explore in conjunction to motion.
January 2019	***Schedule defense meeting for March 2019.** Analyze associations between motion and clinical variables. Write paper on age-based patterns of motion, descriptions of motion, and quantification of motion.
February 2019	Finish any remaining analyses Outline paper on clinical variables and motion patterns Revise dissertation
March 2019	Write paper on clinical variables and motion patterns ***Defend dissertation.**

BIBLIOGRAPHY

[Aksoy et al., 2008] Aksoy, M., Newbould, R., Straka, M., Holdsworth, S. J., Skare, S. T., Santos, J. M., and Bammer, R. (2008). A Real Time Optical Motion Correction System Using a Single Camera and 2D Marker. *Proceedings of the 16th Scientific Meeting of ISMRM*, 16:3120.

[Alexander, 2012] Alexander, M. (2012). Managing Patient Stress in Pediatric Radiology. *Radiologic Technology*, 83(6):549–560.

[Assaf et al., 2010] Assaf, M., Jagannathan, K., Calhoun, V. D., Miller, L., Stevens, M. C., Sahl, R., O'Boyle, J. G., Schultz, R. T., and Pearlson, G. D. (2010). Abnormal functional connectivity of default mode sub-networks in autism spectrum disorder patients. *NeuroImage*, 53(1):247–256.

[Avants et al., 2014] Avants, B. B., Tustison, N. J., Stauffer, M., Song, G., Wu, B., and Gee, J. C. (2014). The Insight ToolKit image registration framework. *Frontiers in Neuroinformatics*, 8(April).

[Ayres, 1920] Ayres, L. P. (1920). The correlation ratio. *The Journal of Educational Research*, 2(1):452–456.

[Barnea-Goraly et al., 2014] Barnea-Goraly, N., Weinzimer, S. A., Ruedy, K. J., Mauras, N., Beck, R. W., Marzelli, M. J., Mazaika, P. K., Aye, T., White, N. H., Tsalikian, E., Fox, L., Kollman, C., Cheng, P., and Reiss, A. L. (2014). High success rates of sedation-free brain MRI scanning in young children using simple subject preparation protocols with and without a commercial mock scanner - the Diabetes Research in Children Network (DirecNet) experience. *Pediatric Radiology*, 44(2):181–186.

[Beckmann and Smith, 2004] Beckmann, C. F. and Smith, S. M. (2004). Probabilistic Independent Component Analysis for Functional Magnetic Resonance Imaging. *IEEE Transactions on Medical Imaging*, 23(2):137–152.

[Behzadi et al., 2007] Behzadi, Y., Restom, K., Liau, J., and Liu, T. T. (2007). A component based noise correction method (CompCor) for BOLD and perfusion based fMRI. *NeuroImage*, 37(1):90–101.

[Bharatha et al., 2001] Bharatha, A., Hirose, M., Hata, N., Warfield, S. K., Ferrant, M., Zou, K. H., Suarez-Santana, E., Ruiz-Alzola, J., D'Amico, A., Cormack, R. A., Kikinis, R., Jolesz, F. A., and Tempany, C. M. (2001). Evaluation of three-dimensional finite element-based deformable registration of pre- and intraoperative prostate imaging. *Medical Physics*, 28(12):2551–60.

[Coté and Wilson, 2016] Coté, C. J. and Wilson, S. (2016). Guidelines for Monitoring and Management of Pediatric Patients Before, During, and After Sedation for Diagnostic and Therapeutic Procedures: Update 2016. *Pediatrics*.

[Dewey et al., 2007] Dewey, M., Schink, T., and Dewey, C. F. (2007). Claustrophobia during magnetic resonance imaging: Cohort study in over 55,000 patients. *Journal of Magnetic Resonance Imaging*, 26(5):1322–1327.

[Dice, 1945] Dice, L. R. (1945). Measures of the Amount of Ecologic Association Between Species. *Ecology*, 26(3):297–302.

[Dosenbach et al., 2017] Dosenbach, N. U., Koller, J. M., Earl, E. A., Miranda-Dominguez, O., Klein, R. L., Van, A. N., Snyder, A. Z., Nagel, B. J., Nigg, J. T., Nguyen, A. L., Wesevich, V., Greene, D. J., and Fair, D. A. (2017). Real-time motion analytics during brain MRI improve data quality and reduce costs. *NeuroImage*, 161(January):80–93.

[Forman et al., 2011] Forman, C., Aksoy, M., Hornegger, J., and Bammer, R. (2011). Self-encoded marker for optical prospective head motion correction in MRI. *Medical Image Analysis*, 15(5):708–719.

[Fox et al., 2015] Fox, C. K., Sidney, S., and Fullerton, H. J. (2015). Community-based case–control study of childhood stroke risk associated with congenital heart disease. *Stroke*, 46(2):336–340.

[Friston et al., 1995] Friston, K. J., Ashburner, J., Frith, C. D., Poline, J. ., Heather, J. D., and Frackowiak, R. S. (1995). Spatial registration and normalization of images. *Human Brain Mapping*, 3(3):165–189.

[Friston et al., 1996] Friston, K. J., Williams, S., Howard, R., Frackowiak, R. S. J., and Turner, R. (1996). Movement-Related effects in fMRI time-series. *Magnetic Resonance in Medicine*, 35(3):346–355.

[Gale et al., 2013] Gale, C., Jeffries, S., Logan, K. M., Chappell, K. E., Uthaya, S. N., and Modi, N. (2013). Avoiding sedation in research MRI and spectroscopy in infants: our approach, success rate and prevalence of incidental finding. *Arch Dis Child Fetal Neonatal Ed*, 98:F267–F268.

[Garcia-Palacios et al., 2007] Garcia-Palacios, A., Hoffman, H. G., Richards, T. R., Seibel, E. J., and Sharar, S. R. (2007). Use of Virtual Reality Distraction to Reduce Claustrophobia Symptoms during a Mock Magnetic Resonance Imaging Brain Scan: A Case Report. *CyberPsychology and Behavior*, 10(3):485–488.

[Gorgolewski et al., 2011] Gorgolewski, K., Burns, C. D., Madison, C., Clark, D., Halchenko, Y. O., Waskom, M. L., and Ghosh, S. S. (2011). Nipype : a flexible , lightweight and extensible neuroimaging data processing framework in Python. *Frontiers in Neuroinformatics*, 5(August).

[Greicius et al., 2003] Greicius, M. D., Krasnow, B., Reiss, A. L., and Menon, V. (2003). Functional connectivity in the resting brain: A network analysis of the default mode hypothesis. *Proceedings of the National Academy of Sciences of the United States of America*, 100(1):253–258.

[Harned and Strain, 2001] Harned, R. K. and Strain, J. D. (2001). MRI-compatible audio / visual system : impact on pediatric sedation. *Pediatric Radiology*, pages 247–250.

[Jenkinson et al., 2002] Jenkinson, M., Bannister, P., Brady, M., and Smith, S. (2002). Improved Optimization for the Robust and Accurate Linear Registration and Motion Correction of Brain Images. *NeuroImage*, 17:825–841.

[Jenkinson and Smith, 2001] Jenkinson, M. and Smith, S. (2001). A global optimisation method for robust affine registration of brain images. *Medical Image Analysis*, 5:143–156.

[Jo et al., 2013] Jo, H. J., Gotts, S. J., Reynolds, R. C., Bandettini, P. A., Martin, A., Cox, R. W., and Saad, Z. S. (2013). Effective preprocessing procedures virtually eliminate distance-dependent motion artifacts in resting state FMRI. *Journal of Applied Mathematics*, 2013.

[Jo et al., 2010] Jo, H. J., Saad, Z. S., Simmons, W. K., Milbury, L. A., and Cox, R. W. (2010). Mapping sources of correlation in resting state FMRI, with artifact detection and removal. *NeuroImage*, 52(2):571–582.

[Khalil et al., 1994] Khalil, A., Aggarwal, R., Thirupuram, S., and Arora, R. (1994). Incidence of Congenital Heart Disease Among Hospital Live Births in India. *Journal of Indian Pediatrics*, 31:519–527.

[Khan et al., 2007] Khan, J. J., Donnely, L. F., Koch, B. L., Curtwright, L. A., Dickerson, J. M., Hardin, J. L., Hutchinson, S., Wright, J., and Gessner, K. E. (2007). A program to decrease the need for pediatric sedation for CT and MRI. *Applied Radiology*, April:30–33.

[KinetiCor Biometric Intelligence, 2019] KinetiCor Biometric Intelligence (2019). The kineticor platform.

[Liao et al., 2005] Liao, R., Krolik, J. L., and McKeown, M. J. (2005). An information-theoretic criterion for intrasubject alignment of FMRI time series: Motion corrected independent component analysis. *IEEE Transactions on Medical Imaging*, 24(1):29–44.

[Liao et al., 2016] Liao, R., Turk, E. A., Zhang, M., Luo, J., Ellen Grant, P., Adalsteinsson, E., and Golland, P. (2016). Temporal registration in in-utero volumetric MRI time

series. *Lecture Notes in Computer Science (including subseries Lecture Notes in Artificial Intelligence and Lecture Notes in Bioinformatics)*, 9902 LNCS:54–62.

[Maclaren et al., 2013] Maclaren, J., Herbst, M., Speck, O., and Zaitsev, M. (2013). Prospective motion correction in brain imaging: A review. *Magnetic Resonance in Medicine*, 69(3):621–636.

[Malviya et al., 2000] Malviya, S., Voepel-Lewis, T., Prochaska, G., and Tait, A. R. (2000). Prolonged Recovery and Delayed Side Effects of Sedation for Diagnostic Imaging Studies in Children. *Pediatrics*, 105(3).

[Mathur et al., 2008] Mathur, A. M., Neil, J. J., McKinstry, R. C., and Inder, T. E. (2008). Transport, monitoring, and successful brain MR imaging in unsedated neonates. *Pediatric Radiology*, 38(3):260–264.

[Mebius et al., 2017] Mebius, M. J., Kooi, E. M., Bilardo, C. M., and Bos, A. F. (2017). Brain Injury and Neurodevelopmental Outcome in Congenital Heart Disease: A Systematic Review. *Pediatrics*, 140(1):e20164055.

[Mozaffarian et al., 2016] Mozaffarian, D., Benjamin, E. J., Go, A. S., Arnett, D. K., Blaha, M. J., Cushman, M., Das, S. R., Ferranti, S. D., Després, J.-p., Fullerton, H. J., Howard, V. J., Huffman, M. D., Isasi, C. R., Jiménez, M. C., Judd, S. E., Kissela, B. M., Lichtman, J. H., Lisabeth, L. D., Liu, S., Mackey, R. H., Magid, D. J., McGuire, D. K., Mohler, E. R., Moy, C. S., Muntner, P., Mussolino, M. E., Nasir, K., Neumar, R. W., Nichol, G., Palaniappan, L., Pandey, D. K., Reeves, M. J., Rodriguez, C. J., Rosamond, W., Sorlie, P. D., Stein, J., Towfighi, A., Turan, T. N., Virani, S. S., Woo, D., Yeh, R. W., and Turner, M. B. (2016). *Heart Disease and Stroke Statistics 2016 Update A Report From the American Heart Association*. American Heart Association.

[Murphy and Brunberg, 1997] Murphy, K. J. and Brunberg, J. A. (1997). Adult claustrophobia, anxiety and sedation in MRI. *Magnetic Resonance Imaging*, 15(1):51–54.

[Nikyar et al., 2011] Nikyar, B., Sedehi, M., Mirfazeli, A., Qorbani, M., and Golalipour, M.-J. (2011). Prevalence and Pattern of Congenital Heart Disease among Neonates in Gorgan, Northern Iran (2007-2008). *Iranian Journal of Pediatrics*, 21(3):307–12.

[Parkes et al., 2017] Parkes, L., Fulcher, B. D., Yucel, M., and Fornito, A. (2017). An evaluation of the efficacy, reliability, and sensitivity of motion correction strategies for resting-state functional MRI. *bioRxiv*.

[Patel et al., 2014] Patel, A. X., Kundu, P., Rubinov, M., Jones, P. S., Vértes, P. E., Ersche, K. D., Suckling, J., and Bullmore, E. T. (2014). A wavelet method for modeling and despiking motion artifacts from resting-state fMRI time series. *NeuroImage*, 95:287–304.

[Patriat et al., 2017] Patriat, R., Reynolds, R. C., and Birn, R. M. (2017). An improved model of motion-related signal changes in fMRI. *NeuroImage*, 144:74–82.

[Power et al., 2012] Power, J. D., Barnes, K. A., Synder, A. Z., Schlagger, B. L., and Petersen, S. E. (2012). Spurious but systematic correlations in functional connectivity MRI networks arise from subject motion. *NeuroImage*, 59(3):2142–2154.

[Power et al., 2014] Power, J. D., Mitra, A., Laumann, T. O., Snyder, A. Z., Schlaggar, B. L., and Petersen, S. E. (2014). Methods to detect, characterize, and remove motion artifact in resting state fMRI. *NeuroImage*, 84:320–341.

[Power et al., 2015] Power, J. D., Schlaggar, B. L., and Petersen, S. E. (2015). Recent progress and outstanding issued in motion correction resting state fmri. *NeuroImage*, 105:536–551.

[Pruim et al., 2015] Pruim, R. H., Mennes, M., van Rooij, D., Llera, A., Buitelaar, J. K., and Beckmann, C. F. (2015). ICA-AROMA: A robust ICA-based strategy for removing motion artifacts from fMRI data. *NeuroImage*, 112:267–277.

[Qu et al., 2016] Qu, Y., Liu, X., Zhuang, J., Chen, G., Mai, J., Guo, X., Ou, Y., Chen, J., Gong, W., Gao, X., Wu, Y., and Nie, Z. (2016). Incidence of Congenital Heart Disease: The 9-Year Experience of the Guangdong Registry of Congenital Heart Disease, China. *PLOS ONE*, 11(7):e0159257.

[Rahim et al., 2008] Rahim, F., Ebadi, A., Saki, G., and Remazani, A. (2008). Prevalence of Congenital Heart Disease in Iran: A Clinical Study. *Journal of Medical Sciences(Faisalabad)*, 8(6):547–552.

[Raichle et al., 2001] Raichle, M. E., MacLeod, A. M., Snyder, A. Z., Powers, W. J., Gusnard, D. A., and Shulman, G. L. (2001). A default mode of brain function. *Proceedings of the National Academy of Sciences*, 98(2):676–682.

[Roche et al., 1998a] Roche, A., Malandain, G., Ayache, N., and Pennec, X. (1998a). *Multimodal image registration by maximization of the correlation ratio*. PhD thesis, INRIA.

[Roche et al., 1998b] Roche, A., Malandain, G., Pennec, X., and Ayache, N. (1998b). The correlation ratio as a new similarity measure for multimodal image registration. *Proceedings of MICCAI*, pages 1115–1124.

[Rugg, 1917] Rugg, H. O. (1917). *Statistical methods applied to education: A textbook for students of education in the quantitative study of school problems*. Houghton Mifflin.

[Rutman, 2009] Rutman, M. S. (2009). Sedation for emergent diagnostic imaging studies in pediatric patients. *Current Opinion in Pediatrics*, 21(3):306–312.

[Salimi-Khorshidi et al., 2014] Salimi-Khorshidi, G., Douaud, G., Beckmann, C. F., Glasser, M. F., Griffanti, L., and Smith, S. M. (2014). Automatic denoising of functional MRI data: Combining independent component analysis and hierarchical fusion of classifiers. *NeuroImage*, 90:449–468.

[Satterthwaite et al., 2013] Satterthwaite, T. D., Elliott, M. A., Gerraty, R. T., Ruparel, K., Loughead, J., Calkins, M. E., Eickhoff, S. B., Hakonarson, H., Gur, R. C., Gur, R. E., and Wolf, D. H. (2013). An improved framework for confound regression and filtering for control of motion artifact in the preprocessing of resting-state functional connectivity data. *NeuroImage*, 64(1):240–256.

[Satterthwaite et al., 2012] Satterthwaite, T. D., Wolf, D. H., Loughead, J., Ruparel, K., Elliott, M. A., Hakonarson, H., Gur, R. C., and Gur, R. E. (2012). Impact of In-Scanner Head Motion on Multiple Measures of Functional Connectivity: Relevance for Studies of Neurodevelopment in Youth. *NeuroImage*, 60(1):623–632.

[Saxena, 2005] Saxena, A. (2005). Congenital Heart Disease in India: A Status Report. *Indian Journal of Pediatrics*, 72(7):595–598.

[Shah et al., 2008] Shah, G., Singh, M., Pandey, T., Kalakheti, B., and Bhandari, G. (2008). Incidence of congenital heart disease in tertiary care hospital. *Kathmandu University Medical Journal*, 6(1):33–36.

[Smyser et al., 2010] Smyser, C. D., Inder, T. E., Shimony, J. S., Hill, J. E., Degnan, A. J., Snyder, A. Z., and Neil, J. J. (2010). Longitudinal analysis of neural network development in preterm infants. *Cerebral Cortex*, 20(12):2852–2862.

[Smyser and Neil, 2015] Smyser, C. D. and Neil, J. J. (2015). Use of resting state functional MRI to study brain development and injury in neonates. *Seminars in Perinatology*, 39(2):130–140.

[TracInnovations, 2019] TracInnovations (2019). Tracinnovations mri markerless motion tracker and monitor system.

[United States Food and Drug Administration, 2016] United States Food and Drug Administration (2016). Drug Safety and Availability - FDA Drug Safety Communication: FDA review results in new warnings about using general anesthetics and sedation drugs in young children and pregnant women. Technical report, United States Food and Drug Administration.

[van der Linde et al., 2011] van der Linde, D., Konings, E. E., Slager, M. A., Witsenburg, M., Helbing, W. A., Takkenberg, J. J., and Roos-Hesselink, J. W. (2011). Birth Prevalence of Congenital Heart Disease Worldwide. *Journal of the American College of Cardiology*, 58(21):2241–2247.

[van Dijk et al., 2012] van Dijk, K. R., Sabuncu, M. R., and Buckner, R. L. (2012). The influence of head motion on intrinsic functional connectivity MRI. *NeuroImage*, 59(1):431–438.

[Webb et al., 2015] Webb, G., Mulder, B. J., Aboulhosn, J., Daniels, C. J., Elizari, M. A., Hong, G., Horlick, E., Landzberg, M. J., Marelli, A. J., O'Donnell, C. P., Oechslin, E. N., Pearson, D. D., Pieper, E. P., Saxena, A., Schwerzmann, M., Stout, K. K., Warnes,

C. A., and Khairy, P. (2015). The care of adults with congenital heart disease across the globe: Current assessment and future perspective: A position statement from the International Society for Adult Congenital Heart Disease (ISACHD). *International Journal of Cardiology*, 195:326–333.

[Windram et al., 2011] Windram, J. D., Grosse-Wortmann, L., Shariat, M., Greer, M.-L., and Yoo, S.-J. (2011). The Feed and Sleep method: how to perform a cardiac MRI in the 1st year of life without the need for General Anesthesia. *Journal of Cardiovascular Magnetic Resonance*, 13(Suppl 1):P224.

[Yan et al., 2013a] Yan, C. G., Cheung, B., Kelly, C., Colcombe, S., Craddock, R. C., Di Martino, A., Li, Q., Zuo, X. N., Castellanos, F. X., and Milham, M. P. (2013a). A comprehensive assessment of regional variation in the impact of head micromovements on functional connectomics. *NeuroImage*, 76:183–201.

[Yan et al., 2013b] Yan, C.-G., Craddock, R. C., He, Y., and Milham, M. P. (2013b). Addressing head motion dependencies for small-world topologies in functional connectomics. *Frontiers in Human Neuroscience*, 7(December):1–19.

[Zaitsev et al., 2017] Zaitsev, M., Burak, A., LeVan, P., and Knowles, B. R. (2017). Prospective Motion Correction in Functional MRI. *NeuroImage*, pages 33–42.

[Zaitsev et al., 2006] Zaitsev, M., Dold, C., Sakas, G., Hennig, J., and Speck, O. (2006). Magnetic resonance imaging of freely moving objects: prospective real-time motion correction using an external optical motion tracking system. *NeuroImage*, 31(3):1038–1050.

[Zang et al., 2007] Zang, Y. F., Yong, H., Chao-Zhe, Z., Qing-Jiu, C., Man-Qiu, S., Meng, L., Li-Xia, T., Tian-Zi, J., and Yu-Feng, W. (2007). Altered baseline brain activity in children with ADHD revealed by resting-state functional MRI. *Brain and Development*, 29(2):83–91.

[Zhao et al., 2019] Zhao, Q. M., Liu, F., Wu, L., Ma, X. J., Niu, C., and Huang, G. Y. (2019). Prevalence of Congenital Heart Disease at Live Birth in China. *Journal of Pediatrics*, 204:53–58.

[Zijdenbos et al., 1994] Zijdenbos, A. P., Dawant, B. M., Margolin, R. A., and Palmer, A. C. (1994). Morphometric Analysis of White Matter Lesions in MR Images: Method and Validation. *IEEE Transactions on Medical Imaging*, 13(4):716–724.

[Zou et al., 2004] Zou, K. H., Warfield, S. K., Bharatha, A., Tempany, C. M., Kaus, M. R., Haker, S. J., Wells, W. M., Jolesz, F. A., and Kikinis, R. (2004). Statistical Validation of Image Segmentation Quality Based on a Spatial Overlap Index. *Academic Radiology*, 11(2):178–189.